

## Large-scale deformation related to the collision of the Aleutian Arc with Kamchatka

Eric L. Geist and David W. Scholl

U.S. Geological Survey, Menlo Park, California

**Abstract.** The far western Aleutian Island Arc is actively colliding with Kamchatka. Westward motion of the Aleutian Arc is brought about by the tangential relative motion of the Pacific plate transferred to major, right-lateral shear zones north and south of the arc. Early geologic mapping of Cape Kamchatka (a promontory of Kamchatka along strike with the Aleutian Arc) revealed many similarities to the geology of the Aleutian Islands. Later studies support the notion that Cape Kamchatka is the farthest west Aleutian "island" and that it has been accreted to Kamchatka by the process of arc-continent collision. Deformation associated with the collision onshore Kamchatka includes gravimetrically determined crustal thickening and formation of a narrow thrust belt of intensely deformed rocks directly west of Cape Kamchatka. The trend of the thrust faults is concave toward the collision zone, indicating a radial distribution of maximum horizontal compressive stress. Offshore, major crustal faults trend either oblique to the Kamchatka margin or parallel to major Aleutian shear zones. These offshore faults are complex, accommodating both strike-slip and thrust displacements as documented by focal mechanisms and seismic reflection data. Earthquake activity is much higher in the offshore region within a zone bounded to the north by the northernmost Aleutian shear zone and to the west by an apparent aseismic front. Analysis of focal mechanisms in the region indicate that the present-day arc-continent "contact zone" is located directly east of Cape Kamchatka. In modeling the dynamics of the collision zone using thin viscous sheet theory, the rheological parameters are only partially constrained to values of  $n$  (the effective power law exponent)  $\geq 3$  and  $Ar$  (the Argand number)  $\leq 30$ . These values are consistent with a forearc thermal profile of Kamchatka, previously determined from heat flow modeling. The thin viscous sheet modeling also indicates that onshore thrust faulting is a consequence, not only of compressive stresses resulting from the west directed collision, but also of sediment-induced coupling of the subducting Pacific plate.

### Introduction

The intersection between the Kamchatka subduction zone and the Aleutian Arc is commonly thought to be a passive juncture; however, recent studies have shown that plate boundary processes are causing the Aleutian Arc to collide end on with Kamchatka [Watson and Fujita, 1985; Zinkevich et al., 1985; Scholl et al., 1989; Zonenshain et al., 1990; Baranov et al.,

1991]. The orientation of Pacific plate convergence with the Aleutian Arc ranges from subnormal near the Alaska Peninsula to tangential at the westernmost end (Figure 1). Distributed shear across the Aleutian Arc results in westward movement of arc rocks and subsequent collision with the Kamchatka. In addition to these kinematic inferences, other authors [Markov et al., 1969; Watson and Fujita, 1985; Zinkevich et al., 1985; Geist et al., 1994] have noted previously that Cape Kamchatka is both structurally and stratigraphically more akin to the Aleutian Arc than to the rest of Kamchatka. Thus Cape Kamchatka appears to be the westernmost Aleutian "island" and is actively being accreted to the Kamchatka mainland.

Over the past decade a considerable amount of Russian geophysical data has been collected in the region where the Kamchatka and Aleutian Arc intersect. In 1981 the R/V *Vulkanolog* conducted an offshore seismic survey of the Kamchatka-Aleutian region [Seliverstov, 1984, 1987] that complemented earlier surveys of the Kamchatka margin [Buffington, 1973; Gribidenko et al., 1983]. These data provide crucial information about offshore structural trends, especially south of the Aleutian Arc. North of the Aleutian Arc, single-channel seismic reflection data collected by the R/V *Vulkanolog* and R/V *Dmitry Mendeleev* in 1988 and multichannel data collected by the Northwestern Pacific Geological Prospecting Expedition from 1980-1986 have detailed the style and timing of spreading within the Komandorsky Basin [e.g., Muzurov et al., 1989; Baranov et al., 1991]. In addition to the seismic reflection experiments, earthquake focal mechanism studies of the Kamchatka-Aleutian region by Zobin [1990a, b, c, 1991] and Zobin et al. [1990] and numerous seismicity studies, for example, Fedotov et al. [1988, 1990], complement studies of the far western Aleutian Arc performed by Cormier [1975] and Newberry et al. [1986]. Furthermore, compilation of an extensive heat flow database and modeling of the thermal structure in the Kamchatka-Aleutian region is presented by Smirnov and Sugrobov [1980, 1982], Smirnov et al. [1992], Sugrobov and Yanovsky [1993]. Finally, recent paleomagnetic studies have revealed that exotic, Late Cretaceous rocks exposed along the eastern margin of Kamchatka originated hundreds of kilometers to the south of their present position [Kovalenko, 1990; Bazhenov et al., 1992; Heiphetz et al., 1994].

In our study we present further structural evidence and results from earthquake studies that the Aleutian Arc is actively colliding with Kamchatka. More importantly, we use the available geological and geophysical data to analyze the deformation that accompanies the arc-continent collision. Specifically, we document a zone of compressional deformation directly ahead of the collision zone and adjacent zones strike-slip faulting to the north and south, much like the collision between Australia and the Banda island arc [McCaffrey and Abers, 1991].

This paper is not subject to U.S. copyright. Published in 1994 by the American Geophysical Union.

Paper number 94TC00428.

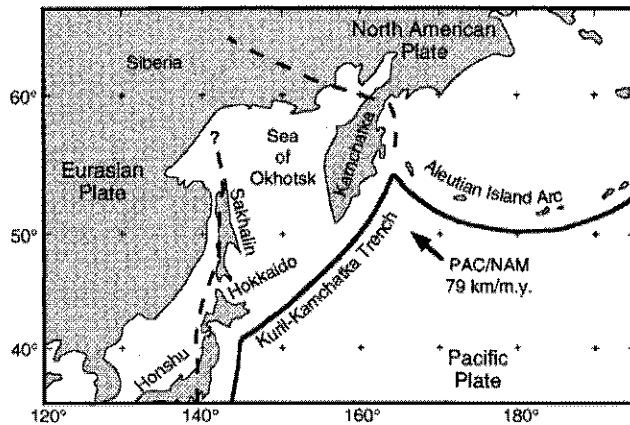


**Figure 1.** Location map for the northeast Asian margin. Arrow indicates direction of Pacific North American relative plate motion (PAC/NAM). Oceanic-continental plate boundaries are shown by thick, solid line; possible boundaries between continental plates shown by dashed lines. Okhotsk plate proposed by *Cook et al.* [1986] and *Riegel et al.* [1993] is located between the two dashed lines. Alternatively, study by *DeMets* [1992] indicates that the North American plate extends to boundary through Japan and Sakhalin Island. Figure is modified from *DeMets* [1992] and *Riegel et al.* [1993].

To understand the dynamics of the collision, we make use of the thin viscous sheet modeling technique. Comparison of model results to the observed deformation provides constraints for the boundary conditions and rheological parameters. The optimal rheology is then interpreted in terms of the first-order temperature structure, determined from heat flow modeling and average strength of the lithosphere in the region.

### Tectonic Setting

In the region of the Kamchatka-Aleutian Arc juncture the Pacific plate is moving 79 km/m.y. in a northwest direction toward Kamchatka and parallel to the trend of the far western Aleutian Arc [*DeMets et al.*, 1990]. The physiography of the Pacific plate includes the northernmost sector of the Hawaiian-Emperor seamount chain. Near the Aleutian Arc there is a counterclockwise bend in the seamount chain such that it is oriented subnormal to the Kamchatka Trench and approximately parallel to the direction of convergence [*Scholl et al.*, 1977]. The sector of the seamount chain north of the bend is termed the Obruchev Swell, which includes Meiji Guyot (Figure 2). Meiji Guyot is flanked to the north by a large thickness of sediment (up to 1.8 km [*Scholl et al.*, 1977]), which we speculate may increase sediment-induced coupling of the northernmost part of the Kamchatka subduction zone. In addition, the incipient subduction of Meiji Guyot is likely to increase stress of the Kamchatka subduction zone at the latitude of Kronotsky Peninsula.

The configuration and motion of the overriding "continental" plates is less certain (Figure 1). The North American plate most likely encompasses the Aleutian Arc, eastern Siberia, and possibly the Kamchatka Peninsula [*Chapman and Solomon*, 1976]. However, *Cook et al.* [1986] and *Riegel et al.* [1993]

identify a separate plate termed the Okhotsk plate, extending from Sakhalin Island to the Kuril-Kamchatka subduction zone and northward to Karaginsky Island. Although the boundaries of the Okhotsk plate are fairly well defined by seismicity, the relative motion between the Okhotsk plate and the North American and Eurasian plates is less certain. The North American-Okhotsk Euler pole of *Cook et al.* [1986] and *Riegel et al.* [1993] results in slight convergence of the two plates from north of the Aleutian Arc to Karaginsky Island (termed the northeast Kamchatka seismic zone). In contrast to their model, *DeMets* [1992] demonstrates that a separate Okhotsk plate is not necessary to explain slip vector orientations along the Kuril-Kamchatka Trench. His preferred model includes the North American plate extending to central Honshu, between Sakhalin Island and the Kuril-Kamchatka trench (Figure 1).

The transform boundary between the Pacific and North American plates along the far western Aleutian Arc is diffuse, extending northward from the Aleutian Trench across the width of the arc to at least the base of its back arc slope. *Ekström and Engdahl* [1989] and *Geist and Scholl* [1992] showed that part of the transcurrent component of relative plate motion is taken up in the overriding plate along the length of the Aleutian Arc. The distributed transcurrent motion is manifested in the central part of the arc by block rotation. In the far western Aleutian Arc the distributed transcurrent motion is manifested by major, arc-parallel shear zones nearly coincident with the Aleutian Trench and bordering both sides of the arc massif (Steller and Beringa fracture zones, Figure 2). These fault zones are mapped using single channel seismic reflection data (see *Seliverstov* [1984, 1987], *Scholl et al.* [1987], and *Baranov et al.* [1991] for track line maps and seismic data). The fault zones are hundreds of kilometers long and truncate basinal reflections on seismic records, characteristic of strike-slip faults. Hypocenters of most of the shallow earthquakes are concentrated about Steller and Beringa fracture zones [*Seliverstov*, 1984]. Moreover, right-lateral, strike-slip motion is corroborated by abundant strike-slip focal mechanisms (Figure 3) [*Newberry et al.*, 1986]. In particular, recent motion of the Beringa fracture zone and localized arc-parallel spreading in the Komandorsky back arc basin provide convincing evidence for westward transport of the Aleutian Arc [*Baranov et al.*, 1991]. Other fracture zones to the north of Beringa fracture zone are associated with extinct NW-SE directed spreading ridges. A localized zone of active spreading, indicated from the single-channel seismic data, also occurs to the south of the Aleutian Arc massif (Steller Basin, Figure 2) (B. V. Baranov, personal communication, 1992).

### Geodynamics of the Collision

We use a diverse suite of existing geological and geophysical data to (1) confirm the collision of the Aleutian Arc with Kamchatka and (2) examine the style and extent of the associated deformation. These data include seismic refraction/reflection data and gravity data, onshore and offshore structural mapping, earthquake seismicity and focal mechanisms, and paleomagnetic studies.

### Deep Crustal Studies

*Marakhanov and Potap'ev* [1981] indicate that the maximum crustal thickness of Kamchatka from deep seismic data is coincident with the Sredinny (central) Range. Between the

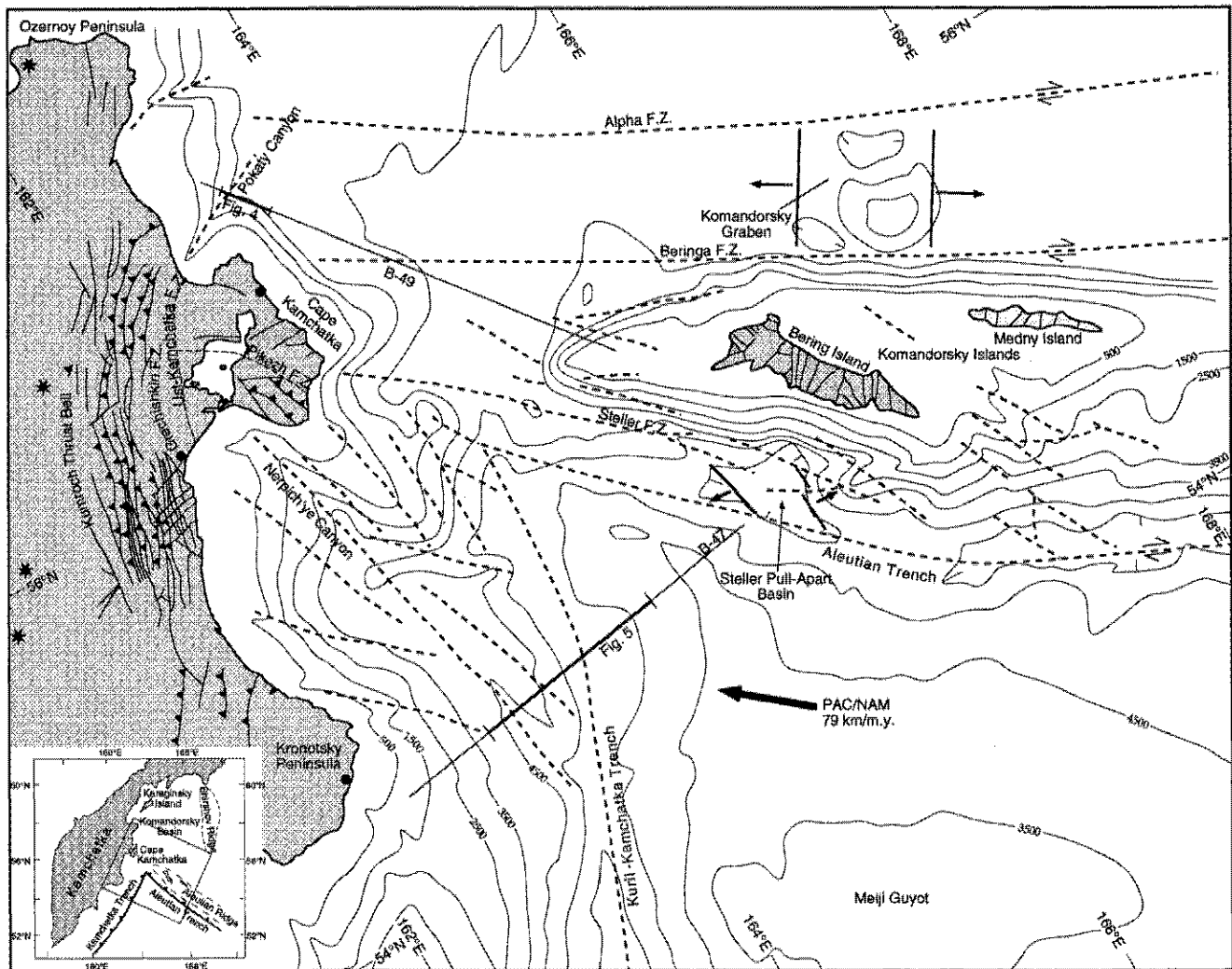


**Figure 2.** Tectonic map of the Cape Kamchatka-Aleutian Arc region. Major onshore faults shown by thin solid lines are compiled from previous mapping by *Markov et al.* [1969], *Marchenko et al.* [1976], *Shapiro* [1980], *Shapiro et al.* [1984], *Borsuk et al.* [1985], *Zinkevich et al.* [1985], *Tsukanov and Zinkevich* [1987], and *Tsukanov and Fedorchuk* [1989]. Triangles in direction of hanging wall are for established thrust faults. Offshore faults shown by dashed lines are compiled from seismic reflection studies [*Krasny et al.*, 1987; *Seliverstov*, 1984, 1987]. Local areas of extension (i.e., Komandorsky Graben and Steller pull-apart basin) north and south of the Aleutian Arc are annotated by small diverging arrows. Large arrow indicates direction of Pacific-North American plate convergence [*DeMets et al.*, 1990]. Solid circles indicate paleomagnetic sampling localities along the eastern Kamchatka margin [*Bazhenov et al.*, 1992]. Stars indicate active volcanoes. Segments of single-channel seismic line B-49 and B-47 shown in Figures 4 and 5, respectively, are indicated by thick line. Bathymetric interval is 1000 m.

latitude of Cape Kamchatka and Kronotsky Peninsula the maximum crustal thickness of the Sredinny Range is 40 km and of the Eastern Ranges is 35 km. Gravity modeling by *Pavlov and Yunov* [1970] revealed a 50-km-wide zone of significant crustal thickening (approximately 4-5 km) coincident with the Kumroch Range. The region of crustal thickening of the Kumroch Range is also suggested in a regional gravity study by *Belyaevsky and Borisov* [1964]. Furthermore, *Gnibidenko et al.* [1974] suggest that the Kumroch negative gravity anomaly extends northward to the eastern part of Ozernoy Peninsula. Crustal thickening along the Kumroch Range is anomalous compared with the other

Eastern Ranges (Tumrok, Valaginsky, and Ganal) and appears to be related to the collision.

#### Onshore and Offshore Structural Mapping

The Kumroch Range, directly west of Cape Kamchatka, is primarily a thrust belt of intensely deformed rocks, hereafter termed the Kumroch thrust belt (Figure 2). It consists of many SE vergent thrust sheets of Late Cretaceous and Paleogene strata [*Markov et al.*, 1969; *Marchenko et al.*, 1976; *Shapiro*, 1980; *Petrina et al.*, 1983; *Shapiro et al.*, 1984; *Tsukanov and Zinkevich*, 1987; *Tsukanov and Fedorchuk*, 1989]. The sequence

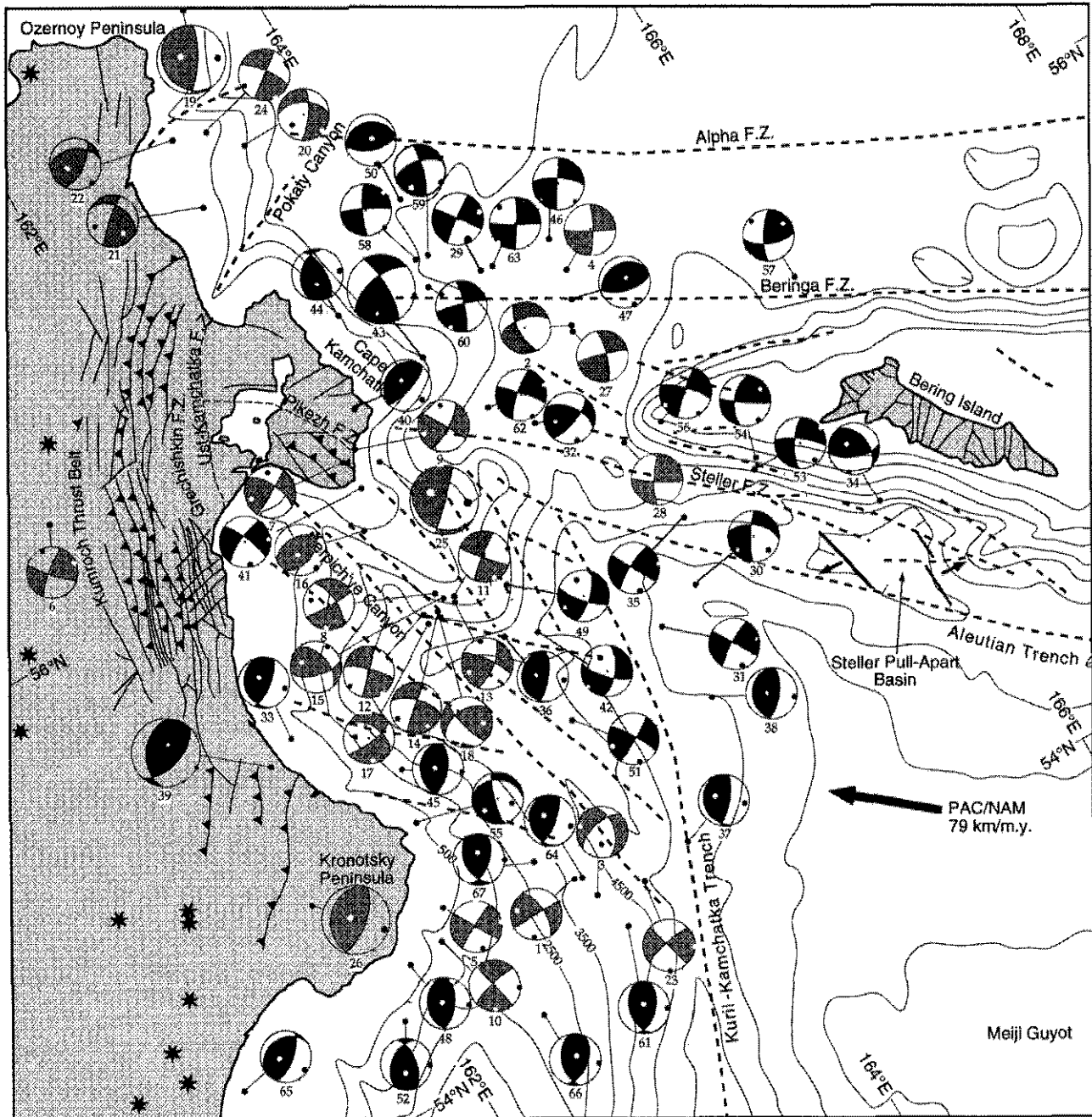


**Figure 3.** Focal mechanisms for earthquakes larger than magnitude 5 in the Cape Kamchatka region from 1964 to 1992. Focal mechanisms shown on lower hemisphere are equal-area projections with compressional quadrants shaded. Focal mechanisms with dark-shaded quadrants represent "best fit" double-couple sources from centroid moment tensor (CMT) solutions; focal mechanisms with light-shaded quadrants derived from body wave analysis. Large-diameter focal mechanisms denote the five largest earthquakes since 1964. Small solid and open circles show orientation of *P* and *T* axes, respectively. See Table 1 for source parameters and references.

of thrusting appears to young to the east as a sequence of underthrust slices [Shapiro *et al.*, 1984; Tsukanov and Zinkevich, 1987]. The easternmost fault bounding the Kumroch thrust belt is thought to be the Grechishkin thrust, formed after middle Miocene time [Shapiro, 1980], although Markov *et al.* [1969] proposed that the concealed Ust-Kamchatka fault zone farther to the east demarcated the eastern boundary of the Kumroch thrust

belt (Figure 2). The trend of faults within the Kumroch thrust belt is concave toward Cape Kamchatka, a pattern suggesting that the thrust belt formed in response to collision of Cape Kamchatka with the Kamchatka mainland. Sparse transverse, strike-slip faulting throughout the Kumroch thrust belt is oriented at angles of 30°-45° to the trend of the thrust faults [Tsikanov and Petrov, 1973; Petrina *et al.*, 1983; Shapiro *et al.*, 1984; Tsukanov and

Zinkevich, 1987; Tsukanov and Fedorchuk, 1989], further indicating that the maximum horizontal compressive stress is approximately normal to the overall trend of faults within the Kumroch thrust belt. Moreover, the sense of displacement on the transverse faults is consistent with collision-induced deformation; predominantly right lateral to the north [Tsukanov and Zinkevich, 1987] and left lateral to the south [Marchenko *et al.*, 1976; Petrina *et al.*, 1983; Shapiro *et al.*, 1984; Tsukanov and Fedorchuk, 1989]. South of Cape Kamchatka and extending across Kronotsky Peninsula, thrust faulting parallels the Kamchatka margin [Shapiro and Seliverstov, 1975; Shapiro, 1980; Petrina *et al.*, 1983; Shapiro *et al.*, 1984]. Similarly, faulting parallels the Kamchatka margin to the north of the Kumroch thrust belt across Ozernoy Peninsula [Marchenko *et al.*, 1976; Zinkevich *et al.*, 1984].

On southern Cape Kamchatka, shallow ENE dipping thrust slices and nappes [Zinkevich *et al.*, 1985] expose Late Cretaceous ophiolitic and island arc rocks. The thrust slices of southern Cape Kamchatka are bounded to the north by the Pikezh fault zone, which may be a westward continuation of the right-lateral shear zone disrupting the Aleutian Arc (Figure 2) [Markov *et al.*, 1969]. Most of the thrust and strike-slip faults on Cape Kamchatka are post-Miocene in age and are most likely related to the arc-continent collision.

Offshore of Cape Kamchatka, fault orientations are generally either oblique to the Kamchatka margin or striking parallel to the NW-SE trending Aleutian shear zones (Figure 2). Most of the faults offset the seafloor and presumably exhibit recent displacement [Seliverstov, 1984, 1987]. The oblique faults, which include the NNW trending faults south of Cape Kamchatka and the NE trending breaks coincident with Pokaty Canyon and an unnamed canyon north of Cape Kamchatka (Figure 4) [Krasny *et al.*, 1987] are most likely strike-slip shears based on their expression in the seismic reflection data and nearby focal mechanisms (Figure 3). The focal planes most closely aligned with the oblique faults south of Cape Kamchatka suggest that the sense of slip is consistently right lateral. Arguably though, post-Miocene thrust faulting mapped on Cape Kamchatka [Markov *et al.*, 1969; Zinkevich *et al.*, 1985] seems to be aligned with the offshore faulting to the south and, with evidence of a reverse component in some of the focal mechanisms, also suggests contractional deformation oblique to the subduction zone in the offshore region. Furthermore, near the Kamchatka Trench, single-channel seismic reflection data indicate that the oblique faults have a thrust component associated with the development of an accretionary wedge (Figure 5). It is apparent therefore that both thrust and strike-slip displacements occur on offshore faults adjacent to the collision zone.

### Seismicity

In the vicinity of a collision zone, earthquakes provide the best indicator of the present-day stress regime. A map of epicenters (magnitude 2 and greater) was compiled from the Soviet "SSR" catalog available from the National Earthquake Information Center's global hypocenter database (Figure 6). Epicenters displayed in Figure 6 are from 1965, after the installation of the Kamchatka seismic station network in the early 1960s [Fedotov *et al.*, 1990], through 1989. Epicenters within the latitude range 54.0°N-58.0°N, longitude range 160°E-164.5°E and hypocentral

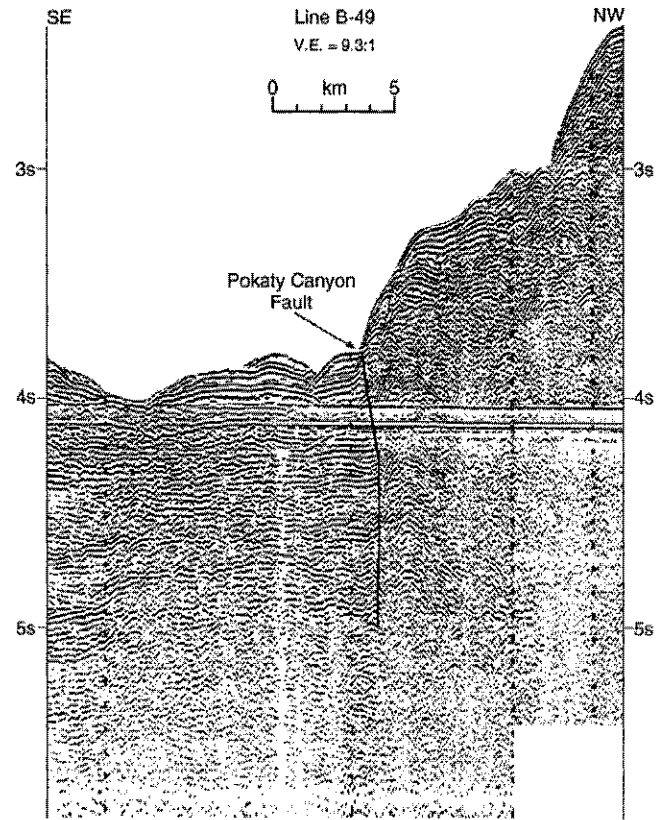


**Figure 4.** Single-channel seismic reflection line B-49 across Pokaty Canyon showing evidence for major fault at base of slope. Data were collected on USNS *Bartlett* in 1970 [Buffington, 1973]. Vertical exaggeration (V.E.) is indicated on figure. See Figure 2 for location.

depths from 0-50 km are included. A 30-s and 15-km radius difference restriction was used in an attempt to eliminate duplicate events.

Most of the earthquakes are concentrated in the offshore region south of Beringa fracture zone and east of an apparent aseismic front. From the data shown in Figure 6 and data from Tarakanov [1987] and Fedotov *et al.* [1988, 1990] the Kamchatka aseismic front is characterized by a sharp decrease in seismicity approximately 130 km inland from the trench, similar to the aseismic front described by Yoshii [1975] and Honda [1985] for the Japan Arc. In Japan, Yoshii [1975] and Honda [1985] also observe that trenchward of the aseismic front, the upper plane of the downgoing slab is characterized by interplate thrust-type earthquakes, whereas arcward of the aseismic front, the upper part of the slab is characterized by within-plate downdip compression. Below about 40 km the Wadati-Benioff zone becomes apparent for the Kamchatka subduction zone south of Cape Kamchatka. In map view the Wadati-Benioff zone between 50 and 200 km bends sharply (30° counterclockwise) north of Kronotsky Peninsula [Fedotov *et al.*, 1988, 1990], correlating with the inland shift of the volcanic axis to the north. We speculate that the bend of the focal zone may be a result of buckling the downgoing Pacific plate at the arc-arc junction.

Locally, concentrations of seismicity occur north of Cape Kamchatka near Pokaty Canyon and an unnamed canyon to the

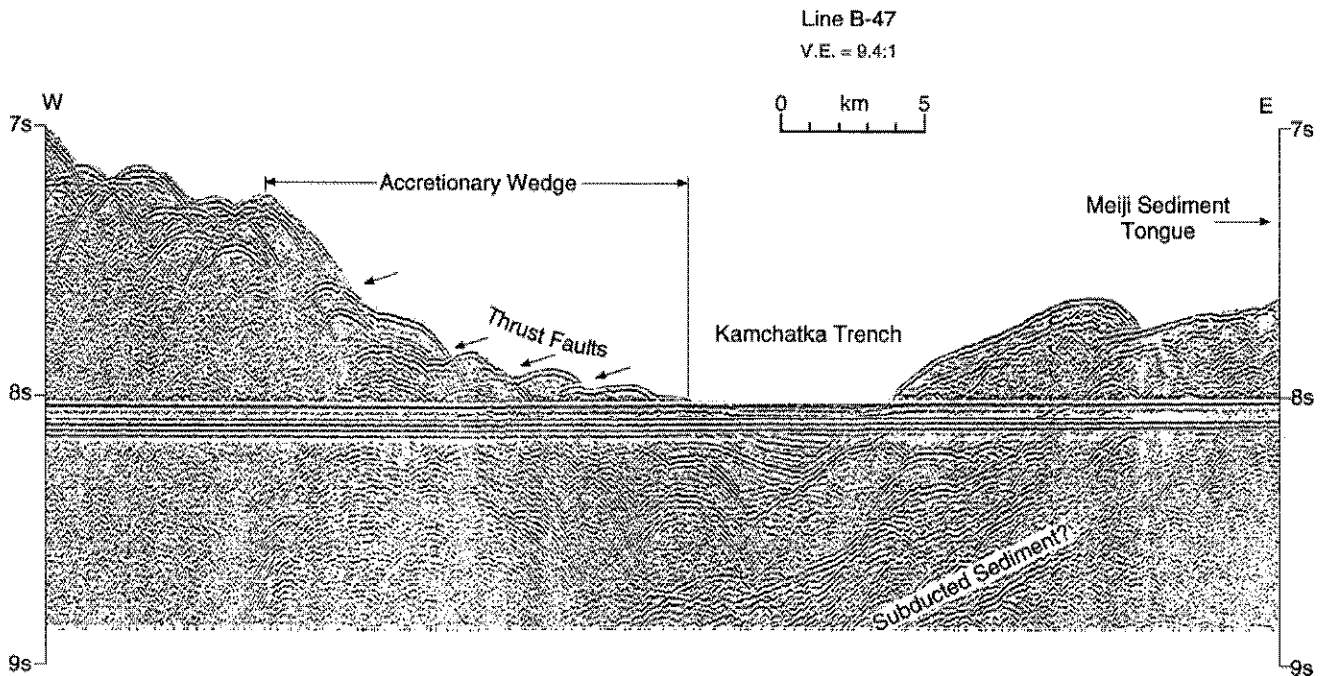


**Figure 5.** Single-channel seismic reflection line B-47 across the northern Kamchatka subduction zone. Data were collected on USNS *Bartlett* in 1970 [Buffington, 1973]. Note evidence for sizable accretionary wedge and thrust faults disrupting the seafloor. Much of the sedimentary deposits from the Meiji sediment tongue appear to be subducted beneath the frontal part of the accretionary wedge. See Figure 2 for location.

north (Figure 4), indicating active faulting in these areas. At the latitude of Kronotsky Peninsula, transverse zones of shallow seismicity (< 50 km) across the width of the Kamchatka Peninsula indicate the presence of large-scale, transverse faulting of the overriding plate [Suprunenko, 1970; Suprunenko et al., 1973; Gordeyev et al., 1992] and, we believe, are related either to extrusion tectonics of the Okhotsk plate or to the incipient subduction of Meiji Guyot.

Landward of the offshore concentration of seismicity, the Kumroch thrust belt is associated with low-level earthquake activity. We interpret that only the frontal part of the collision zone or, conceptually, the contact between the Aleutian Arc and Kamchatka is seismically active. Conversely, deformation related to the collision landward of the contact zone is largely aseismic. Low-level earthquake activity is also coincident with the volcanic axis.

### Focal Mechanisms

Analysis of focal mechanisms of moderate to large earthquakes provides additional information on the present-day stress regime of the region (Figure 3). Table 1 is a catalog of previously published focal mechanisms from 1964-1992. Focal mechanisms of earthquakes from 1964-1977 were determined from body wave first arrivals [Cormier, 1975; Stauder and Mualchin, 1976; Zobin and Simbireva, 1977; Newberry et al., 1986]. From 1977-1992, "best fit" fault plane solutions are from the Harvard centroid moment tensor (CMT) catalog (references for 1977-1991 solutions provided by Dziewonski et al. [1992]). The CMT technique is described by Dziewonski et al. [1981] and Dziewonski and Woodhouse [1983]. The location of earthquakes determined by the CMT technique (centroid coordinates) is

different from the epicenters plotted in the seismicity map of Figure 6; the implications of the shifts in this region are discussed in detail by Zobin [1991]. Also listed in Table 1 is the compensated linear vector dipole (CLVD) ratio ( $f_{clvd}$ ), which is a measure of the deviation from a "pure" double-couple source [Frohlich and Apperson, 1992]. For a pure double-couple source,  $f_{clvd} = 0$ , and for a pure CLVD source,  $f_{clvd} = 0.5$ . Several earthquakes have  $f_{clvd} > 0.30$ , indicating complex source dynamics. Moreover, Zobin [1990b] illustrates that most of the nondouble-couple earthquakes along the Kamchatka subduction zone are concentrated at its terminus with the Aleutian Arc and attributes their origin to curved fault planes.

Focal mechanisms determined for the earthquakes listed in Table 1 vary greatly in the region of the intersection between the Kamchatka and Aleutian Arcs (Table 1 and Figure 3). Several tools are available to analyze the regional stress field from these earthquakes. First, using a technique developed by Frohlich and Apperson [1992] and Frohlich [1992], the principal stress axes are plotted on a ternary graph where the three vertices represent normal, strike-slip, and thrust mechanisms (Figure 7). (The azimuthal gnomonic projection formula listed by Frohlich and Apperson [1992] and Frohlich [1992] contains a misprint. The correct formula [Richardus and Adler, 1972] is used in Figure 7.) The focal mechanisms generally fall in the strike-slip and thrust fields, although there is a significant number of earthquakes that can be classified as "odd" [Frohlich and Apperson, 1992; Frohlich, 1992]. In addition, a contour stereonet plot of the  $P$  axes from all of the earthquakes (Figure 8) indicates at least two azimuthal trends with shallow dip. One trend is in line with the direction of Pacific-North America relative plate motion [DeMets et al., 1990]. The second trend at  $11^\circ$  is approximately parallel to the Kamchatka Trench, while a minor trend at  $340^\circ$  is oblique to

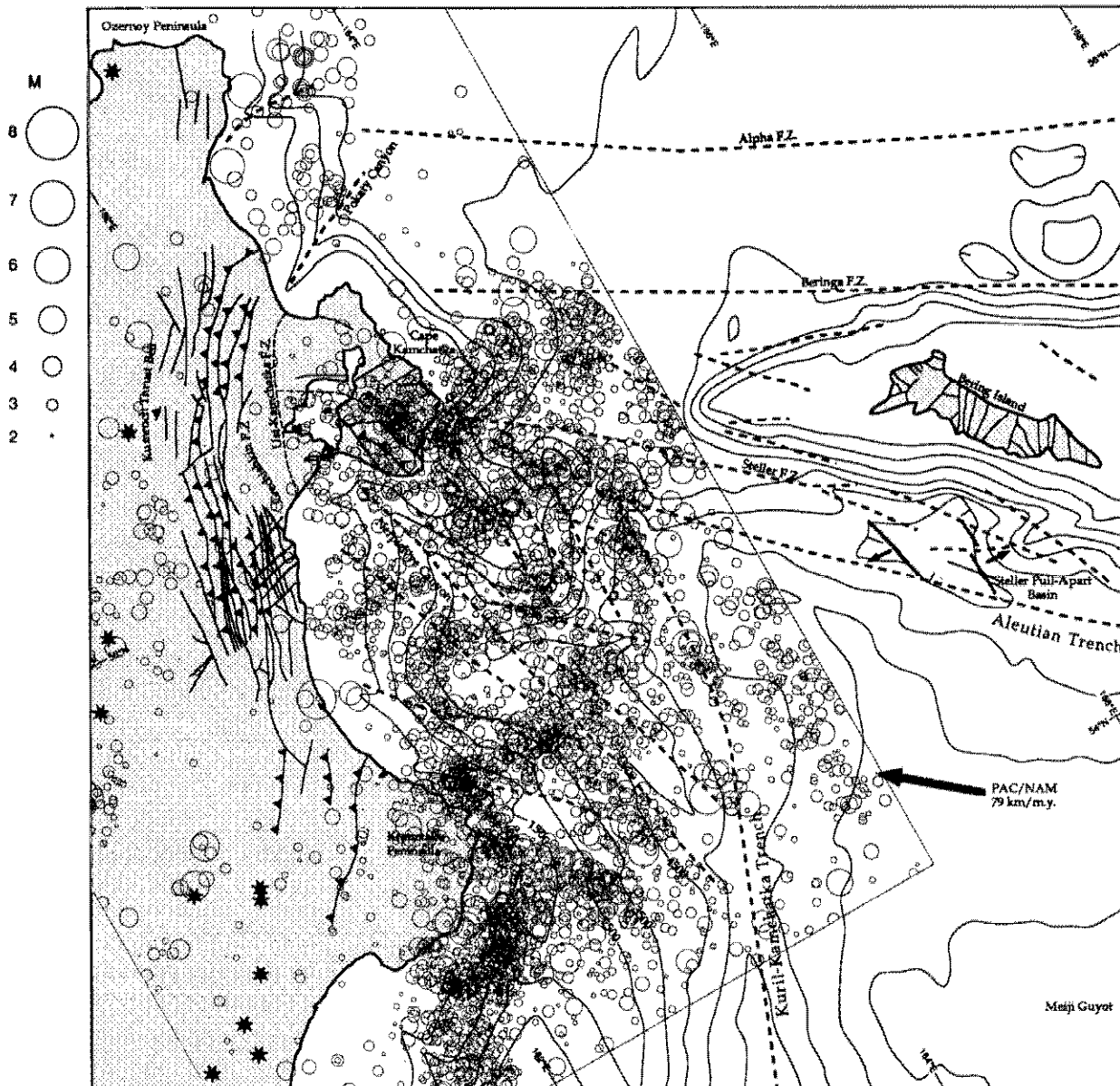


**Figure 6.** Shallow seismicity (0-50 km) for the region near Cape Kamchatka from 1965 to 1990. Earthquakes are magnitude 2 and greater and are located between  $54.0^{\circ}\text{N}$ - $58.00^{\circ}\text{N}$ ,  $160.0^{\circ}\text{E}$ - $164.5^{\circ}\text{E}$ . Radius of circle is proportional to magnitude on a scale of 2-8.

the trench. The diversity of focal mechanisms and multiple trends of  $P$  axes indicate a complex stress regime that cannot be characterized by a single stress tensor. The complexity of the stress field is most likely due to the dynamics of the collision.

The best method of analyzing the seismogenic deformation of this region is to demarcate zones of similar deformation that can, in turn, be related to the kinematics of the collision. Five zones of similar deformation, along with their composite focal mechanisms, are defined in Figure 9. The composite focal mechanisms were calculated by summing the moment tensors (readily available only for CMT solutions) within a given zone. The seismic consistency parameter  $C_s$  of *Frohlich and Apperson* [1992] is a useful measure of the similarity among earthquakes within a specific region. As shown in Table 2, the seismic

consistency for the whole region is low (0.68), but for separate, predefined regions of similar deformation the seismic consistency increases to approximately 1.0, as one would expect.

Zone 1 is a region of right-lateral shearing distributed across the width of the Aleutian Arc, if the NW-SE trending nodal plane corresponding to the trend of major shear zones is interpreted as the fault plane. Alternatively, *Newberry et al.* [1986] propose that left-lateral faulting parallel to the Kamchatka margin can explain these focal mechanisms, although there is no structural evidence of left-lateral transverse shearing of the far western Aleutian Arc. Zone 2 is a region of combined strike-slip faulting and compressional deformation normal to the Kamchatka margin. We interpret this zone as the seismogenic compression zone from the Aleutian Arc-Kamchatka collision. North of Cape

Table 1. Earthquake Coordinates and Source Parameters

Event	Date	Time, UT	Lat, °N	Long, °E	Depth, km	Mag	T Axis		N Axis		P Axis		f <sub>clvd</sub>	Reference
							Az	Pl	Az	Pl	Az	Pl		
1	Nov. 4, 1964	0337	54.44	163.04	5	5.0*	314	20	264	64	220	20		Z
2	Oct. 16, 1965	2001	56.07	164.68	4	5.2*	234	7	333	54	141	36		N, Z
3	July 24, 1965	1145	54.35	163.10	10-20	4.8*	317	5	50	36	222	55		Z
4	July 19, 1966	0140	56.24	164.83	20	5.3*	253	4	144	80	345	9		C, Z
5	Oct. 22, 1966	1247	54.58	162.26	30	5.5*	105	5	320	84	195	5		Z
6	Dec. 14, 1966	0159	56.41	161.28	10-15	4.6*	93	13	297	76	4	2		Z
7	Jan. 8, 1967	0502	56.07	163.06	10-20	5.1*	286	18	143	64	20	18		Z
8	Jan. 8, 1967	0643	55.53	163.14	0-5	5.1*	220	12	102	64	316	24		Z
9	Jan. 8, 1967	0832	56.08	163.17	0-5	4.9*	282	15	145	74	18	15		Z
10	Feb. 6, 1968	0947	54.48	162.16	20	4.8*	214	15	345	70	120	14		Z
11	Jan. 21, 1969	2312	55.48	163.22	10	4.8*	185	3	282	80	96	8		Z
12	Jan. 22, 1969	0042	55.49	163.02	10	5.5*	178	10	58	80	270	10		Z
13	Jan. 22, 1969	0317	55.47	163.21	10	5.0*	280	20	107	68	12	3		Z
14	Jan. 22, 1969	0354	55.47	163.10	10	4.8*	178	25	20	62	275	16		Z
15	Jan. 25, 1969	1210	55.50	163.16	10	4.9*	322	34	130	40	56	6		Z
16	Jan. 26, 1969	1505	55.84	162.93	16	5.5*	266	75	80	16	171	3		C, Z
17	Jan. 29, 1969	0518	55.44	163.03	10	NA	202	18	94	44	310	40		Z
18	Feb. 12, 1969	1539	55.46	163.10	0-10	5.1*	116	40	330	48	222	16		Z
19	Nov. 22, 1969	2310	57.76	163.54	33	7.7 <sup>†</sup>	319	58	209	12	112	29		S,C,Z
20	Dec. 2, 1969	0412	57.18	163.48	0-20	5.1*	160	15	55	45	265	40		Z
21	Dec. 8, 1969	0518	57.07	163.05	0-5	4.6*	170	43	40	40	288	26		Z
22	Dec. 23, 1969	1323	57.32	163.10	33	5.4*	282	58	74	29	170	13		C, Z
23	Feb. 6, 1970	0012	54.31	163.39	40	5.6*	120	8	325	80	210	8		Z
24	June 19, 1970	1853	57.28	163.30	10	5.2*	185	10	52	76	276	10		Z
25	Dec. 15, 1971	0829	56.00	163.26	33	7.8 <sup>†</sup>	336	43	225	16	120	38		S,C,Z
26	March 4, 1973	1758	54.8	161.6	32	6.1*	330	70	227	5	136	20		S
27	Jan. 28, 1975	1153	56.06	164.66	7	5.1*	247	13	92	78	337	2		N
28	April 12, 1977	0354	55.64	164.59	42	5.0*	76	11	270	79	170	3		N
29	Oct. 20, 1977	0818	56.39	164.36	15	5.4 <sup>‡</sup>	98	1	353	84	189	5	0.018	D
30	March 2, 1978	1435	55.10	164.50	15	5.7 <sup>‡</sup>	106	10	322	78	197	7	0.088	D
31	March 3, 1978	1053	55.03	164.21	17	6.0 <sup>‡</sup>	104	4	346	82	194	7	0.015	D
32	Nov. 9, 1979	1345	55.84	164.19	40	5.7 <sup>‡</sup>	292	40	92	49	193	10	0.102	D
33	Nov. 13, 1980	1952	55.34	161.96	49	5.6 <sup>‡</sup>	345	62	227	14	131	24	0.089	D
34	Feb. 9, 1981	1248	55.03	165.71	21	5.5 <sup>‡</sup>	226	13	128	31	336	55	0.011	D
35	May 31, 1982	1021	55.32	164.65	18	6.5 <sup>‡</sup>	265	18	19	51	163	33	0.058	D
36	Nov. 21, 1982	2327	55.29	163.38	10	6.2 <sup>‡</sup>	317	63	216	5	124	26	0.074	D
37	Jan. 5, 1983	0201	54.37	163.72	11	5.8 <sup>‡</sup>	328	62	218	11	123	26	0.010	D
38	Jan. 9, 1983	2104	54.73	164.26	13	6.0 <sup>‡</sup>	316	70	216	4	124	20	0.021	D
39	Aug. 17, 1983	1056	55.30	161.75	77	7.0 <sup>‡</sup>	37	69	239	19	147	7	0.057	D
40	March 26, 1984	2312	56.21	163.26	41	5.4 <sup>‡</sup>	346	62	252	2	160	28	0.056	D
41	Aug. 4, 1984	0912	55.96	163.06	32	5.4 <sup>‡</sup>	110	3	12	70	201	19	0.056	D
42	Nov. 1, 1984	1843	55.23	163.58	10	6.3 <sup>‡</sup>	266	5	167	68	0	31	0.279	D
43	Dec. 28, 1984	1037	56.24	163.80	22	6.7 <sup>‡</sup>	223	32	24	56	127	9	0.264	D
44	Jan. 30, 1985	0324	56.52	163.47	34	5.3 <sup>‡</sup>	226	62	9	23	106	15	0.421	D
45	March 6, 1985	2232	55.05	162.45	43	5.9 <sup>‡</sup>	328	74	216	6	124	14	0.199	D
46	July 29, 1985	0632	56.37	164.82	23	5.6 <sup>‡</sup>	260	10	24	72	167	15	0.077	D
47	Jan. 1, 1986	2210	56.15	164.76	28	5.1 <sup>‡</sup>	338	71	97	9	189	16	0.191	D
48	April 1, 1986	1341	54.46	161.94	47	5.6 <sup>‡</sup>	323	76	211	5	120	13	0.003	D
49	May 2, 1986	1030	55.42	163.53	24	6.1 <sup>‡</sup>	272	3	175	66	3	24	0.348	D
50	Sept. 23, 1986	1141	56.74	164.13	32	5.3 <sup>‡</sup>	14	77	110	1	200	13	0.300	D
51	Jan. 19, 1987	0648	54.92	163.49	36	5.4 <sup>‡</sup>	285	11	96	79	195	2	0.019	D
52	Feb. 14, 1987	1642	54.30	161.73	38	5.5 <sup>‡</sup>	225	65	25	24	118	8	0.106	D
53	July 10, 1987	1850	55.33	165.19	28	6.3 <sup>‡</sup>	79	4	340	67	170	23	0.014	D
54	July 11, 1987	1452	55.37	165.21	39	5.1 <sup>‡</sup>	76	28	295	56	176	18	0.189	D
55	Aug. 12, 1987	0434	54.87	162.36	22	5.2 <sup>‡</sup>	264	30	11	27	134	48	0.101	D
56	Sept. 26, 1987	0531	55.64	164.84	17	5.5 <sup>‡</sup>	273	9	37	74	181	13	0.143	D
57	July 26, 1988	0032	55.82	165.98	15	5.4 <sup>‡</sup>	74	30	239	59	340	6	0.203	D
58	Jan. 27, 1989	0835	56.54	164.05	24	6.3 <sup>‡</sup>	71	4	323	79	162	10	0.140	D
59	April 27, 1989	1040	56.53	164.14	35	5.3 <sup>‡</sup>	242	28	37	59	146	11	0.150	D
60	May 24, 1989	1331	56.42	164.05	44	6.3 <sup>‡</sup>	242	12	73	78	332	2	0.063	D
61	Aug. 30, 1989	0307	54.20	163.18	35	5.5 <sup>‡</sup>	11	74	210	16	119	5	0.303	D

Table 1. (continued)

Event	Date	Time, UT	Lat, °N	Long, °E	Depth, km	Mag	T Axis		N Axis		P Axis		$f_{clvd}$	Reference
							Az	Pl	Az	Pl	Az	Pl		
62	Oct. 15, 1989	0806	55.97	164.00	33	5.2 <sup>‡</sup>	93	6	339	76	185	13	0.131	D
63	June 25, 1990	0719	56.38	164.45	28	5.2 <sup>‡</sup>	256	0	166	84	346	6	0.037	D
64	Dec. 26, 1991	1136	54.42	163.07	15	5.4 <sup>‡</sup>	342	60	228	13	132	27	0.112	D
65	June 19, 1992	0903	54.37	160.69	33	4.9 <sup>‡</sup>	294	65	58	15	153	20	0.384	D
66	July 4, 1992	0326	54.08	162.48	44	5.3 <sup>‡</sup>	30	73	215	17	125	1	0.161	D
67	Nov. 27, 1992	0155	54.57	162.86	15	5.3 <sup>‡</sup>	15	63	210	26	117	6	0.209	D

Abbreviations include lat, latitude; long, longitude; mag, magnitude; az, azimuth, in degrees; pl, plunge, in degrees;  $f_{clvd}$ , compensated linear vector dipole ratio. References are Z, *Zobin and Simbireva* [1977]; N, *Newberry et al.* [1986]; C, *Cormier* [1975]; S, *Stauder and Mualchin* [1976]; D Harvard centroid moment tensor (CMT) database (see *Dziewonski et al.* [1992] for references).

\*Magnitude is  $m_b$ , body wave magnitude.

† $M_s$  is surface wave magnitude.

‡ $M_w$  is moment magnitude.

Kamchatka, zone 3 represents four moderate, offshore strike-slip earthquakes (Figure 3) and concentrations of seismicity coincident with offshore canyons (Figure 6). Zone 4 is a region of strike-slip faulting with right-lateral offset based on the correspondence between mapped faults and NW-SE trending nodal planes. There is some overlap between zones 2 and 4 just south of Cape Kamchatka. Relating these zones to the collision process, there is a significant component of compressional deformation directly east of Cape Kamchatka that is surrounded by zones of strike-slip faulting. In our view, zone 1 indicates westward transport of the Aleutian Arc, whereas zone 2 represents the arc-continent contact, and flanking zones 3 and 4 are regions of strike-slip deformation adjacent to the collision zone. Zone 5, at the latitude of Kronotsky Peninsula, represents a region of reverse and thrust faulting of the overriding plate linked to the incipient subduction of Meiji Guyot (Figure 5).

A similar type of deformation analysis has been performed by *Zobin* [1990a, c, 1991] along the Kamchatka subduction zone, although with significantly different results. Zones 2, 3, and 4 of Figure 9 are included in one zone by *Zobin* [1990a, c, 1991] that is characterized by normal and strike-slip faulting. In addition, his zone that extends along the Aleutian Arc east of Cape Kamchatka is characterized by normal faulting rather than strike-slip faulting as shown in Figure 9. However, farther south along the subduction zone, *Zobin's* results are consistent with thrust and reverse faulting of the upper plate. Earlier studies [*Zobin and Simbireva*, 1977; *Zobin*, 1979] delimit zones that are similar in both extent and style of deformation to the zones shown in Figure 9. *Zobin* [1990a, c] and *Zobin et al.* [1990] also calculate the average strain tensor from the sum of moment tensors over 25-by-25 km square regions. Specifically in the region of Cape Kamchatka, they estimate positive vertical strain rates and shortening parallel to the trend of the Aleutian Arc, consistent with collision-induced stresses and with the above observations.

#### Paleomagnetic Results

Paleomagnetic data from Oligocene to Miocene rocks directly south of Cape Kamchatka (Figure 2) indicate  $49^\circ \pm 13^\circ$  of counterclockwise rotation [*Bazhenov et al.*, 1992]. The sense of rotation is consistent with the dynamics of collision, although a similar amount of rotation is also estimated for middle Eocene samples from farther south on Kronotsky Peninsula.

#### Summary of Deformation Indicators

The previously described geological and geophysical mapping and earthquake studies all indicate that the Aleutian Arc is actively colliding with Kamchatka and that deformation related to the collision extends inland and to the north and south of the collision zone. As indicated by the composite focal mechanisms, the zone of active collision is directly east of Cape Kamchatka (Figure 9), although seismicity indicates that this zone may extend to the Ust-Kamchatka fault zone (Figure 6). This seismogenic zone can be thought of as the contact between the Aleutian Arc and the Kamchatka margin, with deformation related to the collision occurring aseismically inland to the Kumroch Range and seismically offshore to the north and south

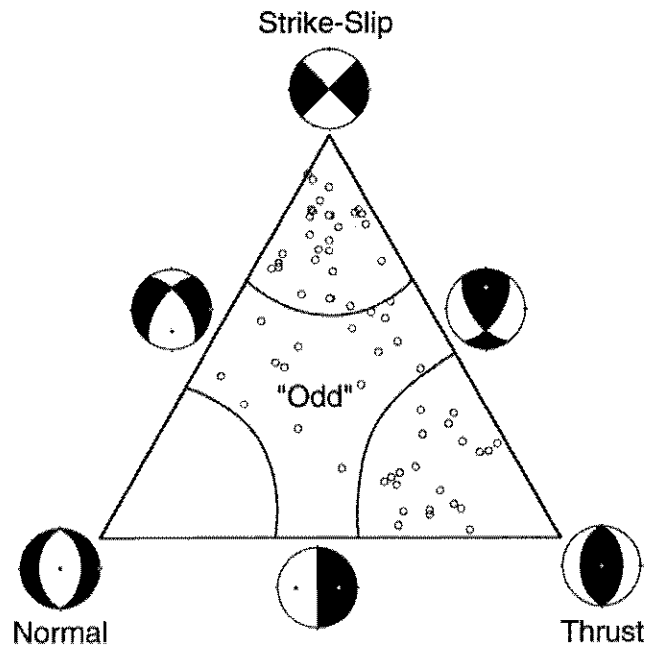
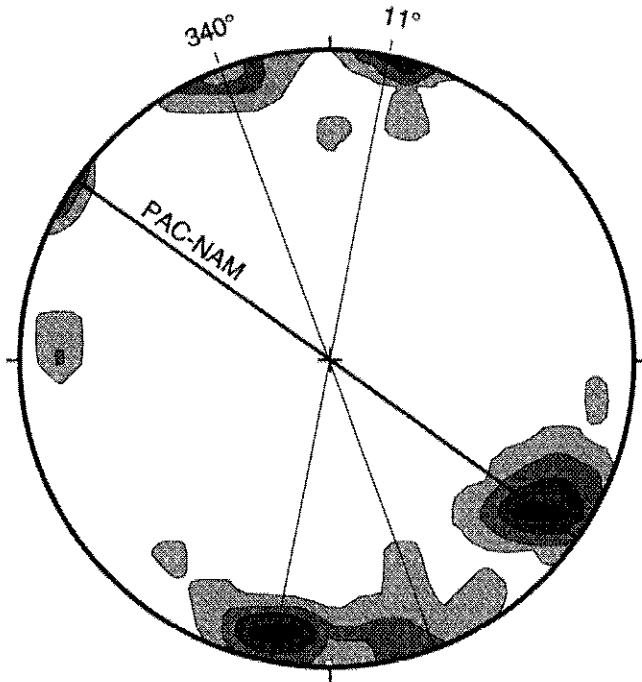


Figure 7. Triangle diagram of earthquakes shown in Figure 3 using method of *Frohlich and Apperson* [1992] and *Frohlich* [1992]. Vertices represent vertical  $T$ ,  $B$ , and  $P$  axes. Strike-slip and normal mechanisms are defined as having  $B$  and  $P$  axes dip  $> 60^\circ$  and thrust mechanisms as having  $T$  axis dip  $> 50^\circ$ . Earthquakes satisfying none of these criteria are defined as "odd."



**Figure 8.** One-percent area contour plot of  $P$  axes from earthquakes shown in Figure 3. Plot is lower hemisphere equal-area projection. Thick line represents trend of Pacific-North American plate convergence. Thin lines indicate two other minor trends. Contour interval is 2% of the total number of earthquakes ( $N=67$ ).

of Cape Kamchatka. Deformation associated with the Aleutian Arc-Kamchatka collision involves (1) uplift and crustal thickening coincident with the Kumroch Range, (2) curvilinear thrust faulting of the Kumroch Range generally concave toward the collision zone, and (3) complex offshore strike-slip faulting with a significant component of shortening oblique to the margin north and south of the collision zone.

### Deformation Modeling

The observed deformation can be related to the dynamics of the arc-continent collision using recently developed continuum models. Although movement along individual faults can not be estimated by continuum modeling, the strain rate tensor and therefore the style of deformation can be determined. In addition, measures of finite strain (e.g., crustal thickening and finite rotation) derived from the modeling can be compared with available field data. We use the thin viscous sheet theory formulated by England and McKenzie [1982, 1983] and Vilotte *et al.* [1982] to study the deformation associated with the arc-continent collision. Previously, this approach has been used extensively to analyze the dynamics of the India-Asia collision zone [Vilotte *et al.*, 1984, 1986; England and Houseman, 1986, 1988, 1989; Houseman and England, 1986], transcurrent plate boundaries [Sonder *et al.*, 1986], continental extension [Sonder and England, 1989], and island arc deformation [Geist and Scholl, 1992; Geist *et al.*, 1993]. A variation of thin sheet modeling has also been employed by Bird [1989] to take into account a stratified or vertically varying rheology, which was

used to study the Laramide orogeny of the western United States [Bird, 1988, 1989]. An additional variation developed by Wdowinski *et al.* [1989] and Wdowinski and O'Connell [1991] uses thin viscous sheet theory coupled with the effects of asthenospheric corner flow to model continental deformation associated with subduction zones.

### Theory

Thin viscous sheet models use a power law constitutive relation and approximate deformation by vertically averaging stress and velocity over the thickness of the lithosphere [England and McKenzie, 1982, 1983; Vilotte *et al.*, 1982]. Forces involved in deforming the lithosphere are tectonic (boundary) forces and buoyancy forces that arise from horizontal gradients in crustal thickness [Artyushkov, 1973]. The two primary model parameters are the effective power law exponent  $n$  and the Argand number  $Ar$ , which is a measure of the vertically averaged strength of the lithosphere [England and McKenzie, 1982; Sonder and England, 1986]. The Argand number is defined as

$$Ar = \frac{g\rho_c(1-\rho_c/\rho_m)L^{(1+1/n)}}{Bu_0^{1/n}} \quad (1)$$

where  $g$  is the gravitational acceleration,  $L$  is the thickness of the lithosphere,  $u_0$  is the characteristic convergence velocity, and  $\rho_c$  and  $\rho_m$  are the crust and mantle densities, respectively.  $B$  is a constant that includes the temperature dependence of rheology averaged throughout the lithosphere, which for a constant geothermal gradient is approximated by

$$B \equiv A \frac{T_M^2 n R}{Q\gamma} \exp\left(\frac{Q}{nRT_M}\right) \quad (2)$$

In this expression,  $A$  is the preexponential constant in the power law relation,  $T_M$  is the Moho temperature,  $R$  is the gas constant,  $Q$  is the activation energy, and  $\gamma$  is the geothermal gradient [England, 1983; Sonder and England, 1989]. Functionally, the Argand number regulates buoyancy forces opposing tectonic forces in deforming the lithosphere. An Argand number of zero indicates that large contrasts in crustal thickness can be sustained and as  $Ar \rightarrow \infty$ , deformation approaches plane horizontal strain [Sonder and England, 1986]. Negative values of  $Ar$ , indicating that buoyancy forces augment rather than oppose the driving forces [Sonder and England, 1989], are not used for this study. The power law exponent  $n$  ranges between 2 and 5 for most crust and mantle rocks [Kirby, 1983; Kirby and Kronenberg, 1987]. Because the rheology is vertically averaged throughout the lithosphere, however, higher values of the effective power law exponent take into account brittle and perfectly plastic behavior of rocks in the upper crust and the upper mantle [Sonder and England, 1986]. Also, Ranalli [1984] and Mackwell [1992] postulate that under specific rheological conditions,  $n$  may be  $< 2$  for rocks in the upper mantle. For these reasons, we test a wide range of  $Ar$  and  $n$  values.

### Boundary Conditions

The boundary of the collision zone is interpreted to the western limit of seismicity in the western part of Cape Kamchatka (Figure 6). The boundary could be farther eastward



**Table 2.** Seismic Consistency and Composite Solutions for Zones of Uniform Deformation

Zone	Number of Focal Mechanisms	Number of CMT Solutions	Seismic Consistency, $C_s$	Composite Solution	
				P Axis Az, Pl	T Axis Az, Pl
Whole region	67	38	0.68	----	----
Zone 1	21	16	0.89	164, 20	257, 8
Zone 2	6	4	1.00	127, 9	223, 33
Zone 3	4	0	----	----	----
Zone 4	13	4	0.98	8, 2	278, 0.4
Zone 5	17	11	0.99	146, 7	35, 70

CMT, centroid moment tensor; az, azimuth, in degrees; pl, plunge, in degrees. See Figure 9 for diagram of zones.

transcurrent velocity of arc rocks is estimated at 35% of the tangential component of relative Pacific plate motion by *Geist and Scholl* [1992] and 60% by *Ekström and Engdahl* [1989] in the central sector of the Aleutian Arc. At the far western end of the Aleutian Arc it is unclear how much of Pacific-North American plate motion is transmitted to westward motion of the arc massif. Also, it is likely that only part of this transcurrent motion is applied at the collision zone, the rest being taken up by subduction beneath Kamchatka. Therefore rather than predefining the velocity of the Aleutian Arc at the collision zone, we adjusted the magnitude of the boundary velocity so that the predicted crustal thickening matched the crustal thickening determined by *Pavlov and Yunov* [1970].

Two sets of boundary conditions are examined (1) zero velocity adjacent to the collision zone and (2) constant velocity south of the collision zone relating to horizontal compression along the Kamchatka subduction zone. It is unlikely that the boundary velocity abruptly increases at the edges of the Aleutian Arc. Therefore a sinusoid shape function is used for the boundary conditions (similar to the boundary conditions specified for ridge subduction by *Geist et al.* [1993]) that represents decreased coupling along the flanks of the Aleutian Arc. Analytically, the boundary conditions are specified as follows:

$$\begin{aligned}
 u(x_0, y) &= u_a \sin\left(y \frac{\pi}{w}\right) & 0 \leq y \leq w & \text{BC set 1} \\
 u(x_0, y) &= u_a \sin\left(y \frac{\pi}{w}\right) & 0 \leq y \leq w & \\
 u(x_0, y) &= \alpha_p u_p & y \leq 0 & \left. \begin{array}{l} \\ \\ \end{array} \right\} \text{BC set 2}
 \end{aligned} \quad (3)$$

where the  $y$  axis is parallel to the Kamchatka subduction zone, the  $x$  axis is parallel to the Aleutian transform boundary,  $w$  is the width of the Aleutian Arc,  $u_a$  is the empirically derived velocity of the far western segment of the Aleutian Arc relative to Kamchatka, and  $u_p$  is the relative convergence of the Pacific plate toward Kamchatka. South of the collision zone for boundary condition (BC) set 2, a proportionality constant ( $\alpha_p$ , analogous to coupling) is used to account for the fact that not all of the Pacific-North America relative velocity is applied to the Kamchatka margin. The values for the parameters described above are given in Table 3, except for  $u_a$  and  $\alpha_p$ , which are given in the figure caption for each model.

The duration of the model is 5 m.y. based on the approximate onset of collision of Cape Kamchatka. The onset of collision is

estimated to be at the end of Miocene time based on movement along the Grechishkin thrust that placed Cretaceous rocks of the Kumroch Range over early to middle Miocene sedimentary deposits [*Markov et al.*, 1969; *Shapiro*, 1980; *Tsukanov and Zinkevich*, 1987]. The collision may have initiated earlier than 5 Ma if the 15 Ma switch from transtensional to transpressional regime along the western Aleutian Arc was caused by the collision [*Yogodzinski et al.*, 1993]. Concurrent with the 5 Ma age, however, accelerated deformation related to increased interplate coupling affected the Aleutian Arc and included block rotation and shearing of the arc massif and compressional deformation of the outer forearc [*Scholl et al.*, 1987; *Geist et al.*, 1988; *Ryan and Scholl*, 1989]. Thus lateral movement of the arc, if not initiated at approximately 5 Ma, accelerated to provide the driving force for the arc-continent collision.

## Results

We first examine the two sets of boundary conditions to determine which best approximates the fault trends of the Kumroch thrust belt. For this test,  $n=3$ , corresponding to the experimentally derived value of  $n$  for most lower crustal and mantle rocks [*Ashby and Verrall*, 1977; *Goetze*, 1978; *Weertman*, 1978; *Brace and Kohlstedt*, 1980; *Karato et al.*, 1986], and  $Ar=10$ , corresponding to the upper limit of optimal values of  $Ar$  determined by *Houseman and England* [1986] for the India-Asia collision. For the first set of boundary conditions (collision only) the maximum horizontal stress axes symmetrically radiate out from the collision zone (Figure 10a). Note that the compressive stress axes are approximately perpendicular to the trend of the faults within the thrust zone to the north, but to the south the correspondence breaks down. The second set of boundary conditions (collision with subduction related compression to the south) results in maximum horizontal compressive stress axes approximately normal to the fault trends both north and south of the collision zone (Figure 10b).

Regions of different styles of faulting are also indicated in Figures 10a and 10b by the two-letter mnemonic as described by *Houseman and England* [1986] and *Bird* [1989]. The first letter denotes the primary style of faulting (N, normal; T, thrust; S, strike slip), with the second letter denoting the secondary style of faulting. For example, NS represents normal faulting with a minor strike-slip component; TT represents thrust faulting parallel to both horizontal principal stress axes. For both sets of boundary conditions the style of deformation includes primary

**Table 3.** Parameters Used in Calculations

	Definition	Value
$w$	width of arc	120 km
$g$	gravitational acceleration	9.8 m s <sup>-2</sup>
$\rho_c$	crust density	2.8 × 10 kg m <sup>-3</sup>
$\rho_m$	mantle density	3.3 × 10 kg m <sup>-3</sup>
$L$	lithosphere thickness	80 km
$T_{BD}$	brittle-ductile temperature	300°C
$R$	gas constant	8.314 J mol <sup>-1</sup> K <sup>-1</sup>
$Q_c$	activation energy for quartz power law flow	2.19 × 10 <sup>5</sup> J mol <sup>-1</sup>
$\gamma_c$	lower crustal geotherm	20°C/km
$\dot{\epsilon}$	strain rate	5.0 × 10 <sup>-16</sup> s <sup>-1</sup>
$A_c$	constant for quartz power law flow	5.0 × 10 <sup>6</sup> s <sup>-1</sup> MPa <sup>-n</sup>
$Q_p$	activation energy for olivine power law flow	5.2 × 10 <sup>5</sup> J mol <sup>-1</sup>
$A_p$	constant for olivine power law flow	7.0 × 10 <sup>4</sup> s <sup>-1</sup> MPa <sup>-n</sup>
$\gamma_p$	mantle geotherm	18°C/km; 20°C/km; 24°C/km*
$T_M$	Moho temperature	650°C; 750°C; 850°C*
$(\sigma_1 - \sigma_3)_{BD}$	stress difference at brittle-ductile transition	240 MPa; 200 MPa; 160 MPa*
$z_{BD}$	depth at brittle-ductile transition	20 km; 15 km; 10 km*

\* First value refers to "cold" lithosphere; second to "normal" lithosphere; third to "hot" lithosphere.

thrust faulting (TS) in front of the collision zone and primary strike-slip faulting (ST) to the north of the collision zone. Unlike the first set of boundary conditions, however, the region to the south of the collision zone for the second set of boundary conditions is characterized by thrust faulting parallel to both principal horizontal stress axes (TT), owing to the combination of compression radiating from the collision zone and the imposed convergent boundary condition related to subduction of the Pacific plate south of the collision zone. As shown previously by the focal mechanism studies (Figure 9), incipient subduction of Meiji Guyot and increased coupling from the large amount of sediment being subducted north of Meiji Guyot, is likely to locally increase compressive stress along the Kamchatka subduction zone. The second set of boundary conditions (a combination of collision and subduction zone coupling to the south) best matches the orientation of faults within the Kumroch thrust belt and thus will be used to further investigate the effects of varying  $n$  and  $Ar$ .

Finite strain indicators (crustal thickening and finite rotation) indicate that deformation is concentrated within approximately 100 km of the collision zone. Figures 10c and 10d are maps of crustal thickness and finite rotation, respectively, for the second set of boundary conditions. As shown in Figure 10c, the collision produces locally thickened crust in front of the collision zone with the maximum crustal thickening located 40 km from the boundary. The finite rotation field (Figure 10d) is calculated by integrating half the vorticity over the duration of the model. This quantity represents the rotation of bodies with small dimensions relative to the deforming medium and is distinguished from the

rotation of material vectors between two points within the medium by *McKenzie and Jackson* [1983]. The bipolar pattern of finite rotation signifies clockwise rotation north of the collision and counterclockwise rotation to the south, with a larger amount of rotation to the north corresponding to the radiating stress field. The predicted sense of finite rotation south of the collision zone (counterclockwise) is the same as that for the paleomagnetic analysis of Oligocene to Miocene rocks in this same region [*Bazhenov et al.*, 1992], although the paleomagnetically measured rotation is much greater than that estimated by the models.

We now vary the effective power law exponent  $n$  to observe how the collision-induced deformation is affected. The effect of increasing  $n$  is to concentrate deformation in regions of highest stress, a phenomenon known as shear thinning [*England and McKenzie*, 1982]. The stress fields (Figure 11) and crustal thickening maps (Figure 12) are calculated for values of  $n$  between 1 and 7. For  $n=1$  the principal compressive stress axes radiate about the collision zone, more so than for  $n=3$  (Figure 11). Also, the dominant style of faulting is strike slip with a minor thrusting component (ST) rather than primary thrust faulting (TS). As  $n$  increases, thrust faulting becomes more predominant. Crustal thickening becomes greater and more compressed near the collision zone with increasing  $n$  (Figure 12). In addition, crustal thinning adjacent north and south of the collision zone is evident for  $n=1, 3$  but not for higher  $n$ . There is little change in the finite rotation field with increasing  $n$  (not shown). Thus increasing  $n$  from 1 to 7 results in a change from diffuse deformation to deformation concentrated near the

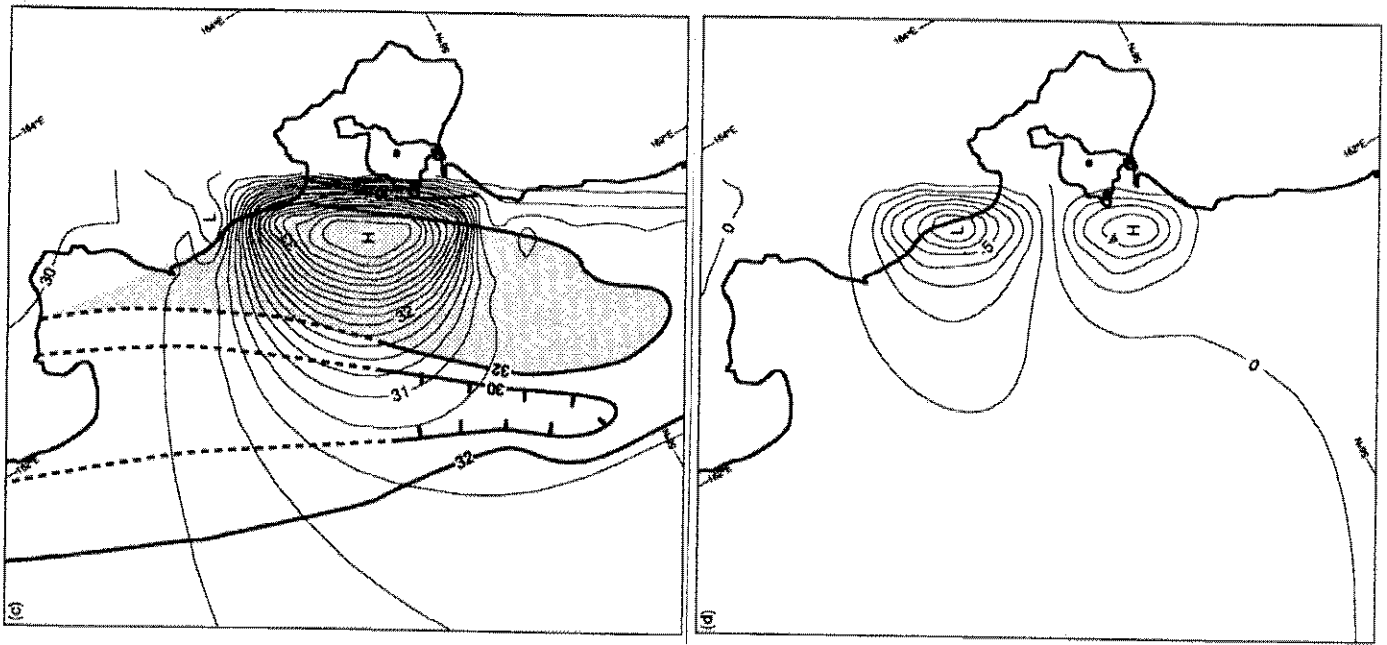


**Figure 10.** Model results after 5 m.y. Magnitude of velocity boundary condition was chosen to best match the amount of observed crustal thickening;  $u_a = 3$  km/m.y.,  $u_p = 79$  km/m.y.,  $\alpha_p = .02$ . (See text for variable definitions.) (a) Principal horizontal stresses for the first set of boundary conditions (collision only) and power law exponent  $n=3$  and Argand number  $A=10$ . Thick axis indicates compressive stress; thin axis indicates tensional stress. Continuous thin line delineates regions with a similar style of faulting derived from the strain rate tensor. The two-letter mnemonic indicates the primary (first letter) and secondary (second letter) style of faulting (T, thrust; S, strike-slip; N, normal). For further explanation, see *Houseman and England* [1986] and *Bird* [1989]. (b) Principal horizontal stresses for the second set of boundary conditions (collision plus subduction-related compression to the south), and  $n=3$  and  $A=10$ . (c) Crustal thickness assuming an initial thickness of 30 km. Contour interval is 0.2 km. Thick contour lines indicate gravimetrically determined crustal thickness [Pavlov and Yunov, 1970]. Lines are dashed where extrapolated based on trends indicated by *Gribudenko et al.* [1974]. (d) Amount of vertical finite rotation measured in degrees (counterclockwise is positive). Contour interval is 2°.

collision zone and from predominantly strike-slip faulting to thrust faulting.

Model results for  $n \geq 3$  are compatible with the trend of thrust faults throughout the Kumroch Range and the lateral extent of crustal thickening. For the case where  $n=1$ , stress magnitudes and orientations are inconsistent with the orientation of thrust faulting in the southern part of the Kumroch thrust belt. Moreover, thrust faulting is secondary to strike-slip faulting for  $n=1$  in the region of the thrust belt. This model also yields a zone of crustal thickening much larger in lateral extent than is predicted by the gravity data [Pavlov and Yunov, 1970; Gribidenko et al., 1974]. For models where  $n \geq 3$ , the maximum horizontal compressive stress is consistently normal to the trend of the thrust faults and the predicted region of crustal thickening is restricted to near the collision zone, consistent with the gravity modeling. Furthermore, as  $n$  increases to 5 and greater, crustal thickening is predicted south of the collision zone, as is also indicated by the gravity data. We interpret that southward extension of the zone of crustal thickening is linked to subduction-related compression. For  $n=3$  the regions of crustal thinning adjacent to the collision zone correlate spatially with Pokaty and Nerpich'ye Canyons. If these canyons are structurally controlled and formed in response to the collision,  $n$  is constrained to a value of 3 because depressions in the crustal thickness do not form for  $n>3$ . However, this is a weak constraint at best. Thus, based on the lateral extent of crustal thickening and stress orientation and magnitude in the southern Kumroch thrust belt, the effective power law exponent can only be constrained to values of 3 or greater.

In a similar manner we vary  $Ar$  and note the corresponding changes in deformation. Increasing  $Ar$  decreases the ability of the lithosphere to sustain crustal thickness contrasts. For the case of the Aleutian Arc-Kamchatka collision the radiating pattern of maximum compressive stress axes becomes more evident as  $Ar$  increases from 0 to 100 (Figure 13). For  $Ar=0$  the maximum compressive stress axes south of the collision zone are oriented normal to the boundary, whereas for  $Ar=100$  these stress axes are highly oblique to the boundary. Moreover, the zone of predominant strike-slip faulting (ST) north of Cape Kamchatka expands southward with increasing  $Ar$ . As expected, the magnitude of crustal thickening in front of the collision zone decreases with increasing  $Ar$  (Figure 14). The finite rotation field does not change appreciably from what is shown in Figure 10d. Thus values of  $Ar$  between 0 and 30 are similar and consistent with the orientation and extent of thrust faulting. For  $Ar > 30$  the extent of dominant strike-slip faulting and the orientation of maximum compressive stress in the southern part of thrust belt are inconsistent with the observed style of deformation.

We are able to model the style and extent of deformation related to the arc-continent collision using thin viscous sheet theory. Values of  $n$  and  $Ar$  are loosely constrained to  $n \geq 3$  and  $Ar \leq 30$ . Whereas, for example, the extent of crustal thickening and style of faulting are well matched with the modeling, the magnitude of finite deformation (crustal thickening and finite rotation) may not be as well estimated. This is related to the fact that modeling finite deformation is dependent on the magnitude of the boundary velocity condition and the duration of its application, both of which are poorly known. Therefore the observed style and extent of faulting, focal mechanisms, and extent (rather than magnitude) of crustal thickening are most useful in evaluating the deformation models.

## Implications for Average Physical Properties of the Lithosphere

The results of the previous section can be interpreted in terms of measurable rock properties following the analyses of England [1983] and Sonder and England [1986]. An equivalent definition of the Argand number is

$$Ar = \frac{g\rho_c(1-\rho_c/\rho_m)L^2\sqrt{2}^{(1/n+1)}}{F_L} \quad (4)$$

written in terms of  $F_L$ , the vertically integrated strength of the lithosphere, rather than the rheological constant  $B$  [Sonder and England, 1986]. In turn,  $F_L$  is estimated by separately estimating the integrated strength of the upper crust ( $F_{UC}$ ), lower crust ( $F_{LC}$ ), and mantle ( $F_M$ ). Expressions for each of these values are derived by England [1983] and Sonder and England [1986] and are given below

$$F_{UC} \cong \frac{1}{2}z_{BD}(\sigma_1 - \sigma_3)_{BD} \quad \bar{\sigma}_n < 200 \text{ MPa} \quad (5)$$

where  $z_{BD}$  is the depth to the brittle-ductile transition and  $\bar{\sigma}_n$  is the effective normal stress on a fault [Byerlee, 1978; Brace and Kohlstedt, 1980];

$$F_{LC} \cong \frac{T_{BD}^2 n_c R}{Q_c \gamma_c} \left( \frac{\dot{\epsilon}}{A_c} \right)^{1/n_c} \exp\left( \frac{Q_c}{n_c RT_{BD}} \right) \quad (6)$$

where  $\dot{\epsilon}$  is the average strain rate,  $T_{BD}$  is the absolute temperature at the brittle-ductile transition,  $\gamma_c$  is the lower crustal geothermal gradient,  $R$  is the gas constant, and  $A_c$ ,  $n_c$ , and  $Q_c$  are constants for the quartz flow law; and

$$F_M \cong \frac{T_M^2 n_p R}{Q_p \gamma_p} \left( \frac{\dot{\epsilon}}{A_p} \right)^{1/n_p} \exp\left( \frac{Q_p}{n_p RT_M} \right) \quad (7)$$

where  $T_M$  is the absolute temperature at the mocho,  $\gamma_p$  is the mantle geothermal gradient, and  $A_p$ ,  $n_p$ , and  $Q_p$  are constants for the olivine flow law. Constants for the above expressions are given in Table 2. We use typical values for  $Q_c$ ,  $Q_p$ ,  $A_c$ , and  $A_p$  from Kirby and Kronenberg [1987]. By using a single value for  $n$  (i.e.,  $n = n_c = n_p$ ) over the thickness of the lithosphere, the relationship between  $n$  and  $Ar$  can be examined (Figure 15). For most lower crustal and mantle rocks, the value of  $n$  ranges between 2 and 5 [Kirby, 1983; Kirby and Kronenberg, 1987], whereas higher values of  $n$  reflect the dominance of low-temperature, high-stress plasticity in the upper mantle [Ashby and Verall, 1977; Tsenn and Carter, 1987] and friction on faults in the upper crust [Sonder and England, 1986]. Three cases are considered based on different possible thermal structures for the lithosphere, labeled "cold," "normal," and "hot" lithosphere in Figure 15. If we fix the temperature at the brittle-ductile transition to 300°C [Sibson, 1984],  $z_{BD}$  can be determined from the thermal structure derived by Smirnov and Sugrovov [1980]

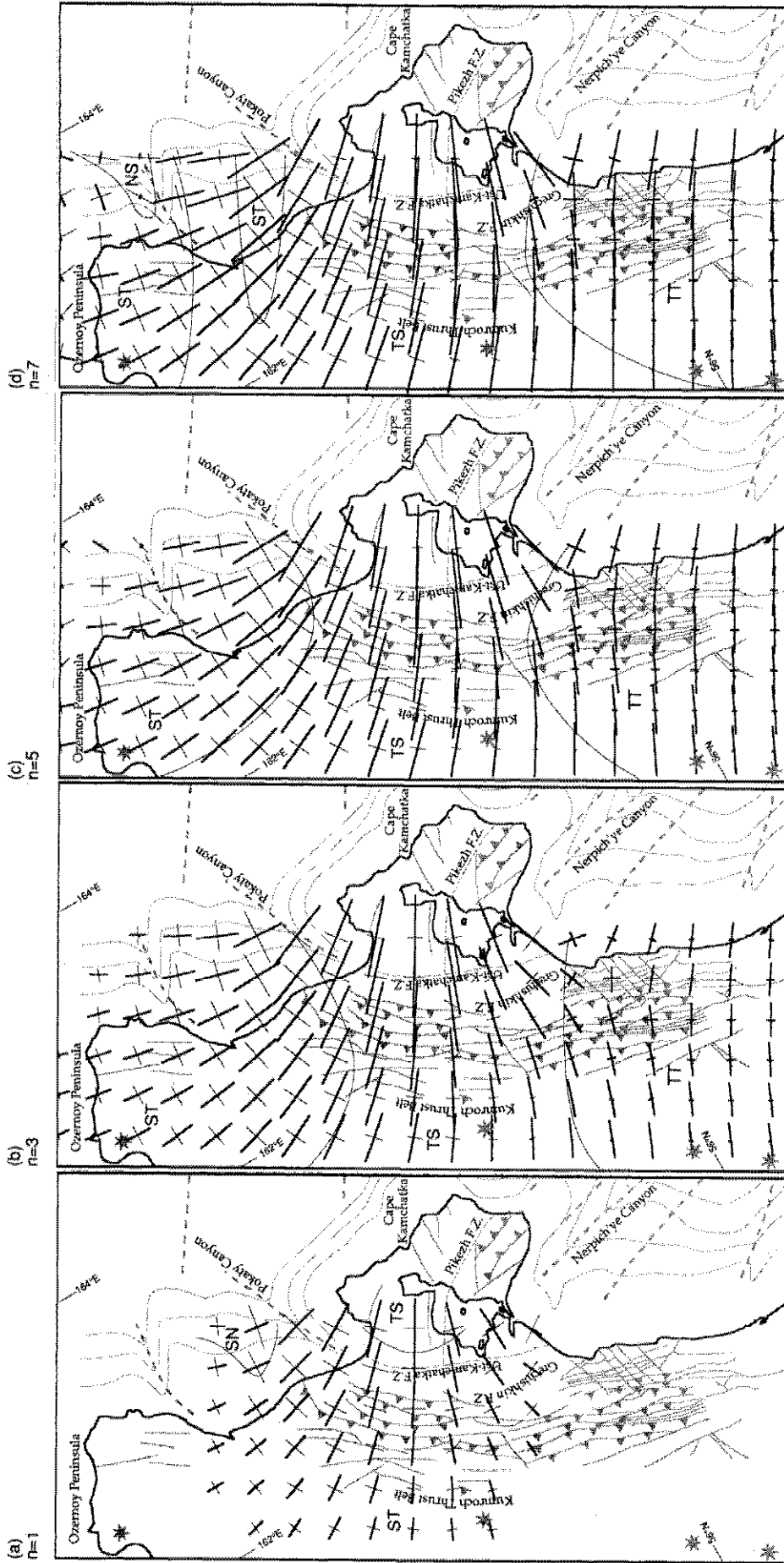


**Figure 11.** Effect on principal horizontal stresses after 5 m.y. by varying  $n$ . Thick axis indicates compressive stress; thin axis indicates tensional stress. Magnitude of velocity boundary condition was chosen to best match the amount of observed crustal thickening. For  $n=1$ ;  $u_d = 5$  km/m.y.,  $\alpha_p = .03$ . For  $n=3$ ;  $u_d = 3$ , km/m.y.  $\alpha_p = .02$ . For  $n=5, 7$ ;  $u_d = 2$  km/m.y.,  $\alpha_p = .01$ . Values are (a)  $n=1$ , (b)  $n=3$ , (c)  $n=5$ , and (d)  $n=7$ .

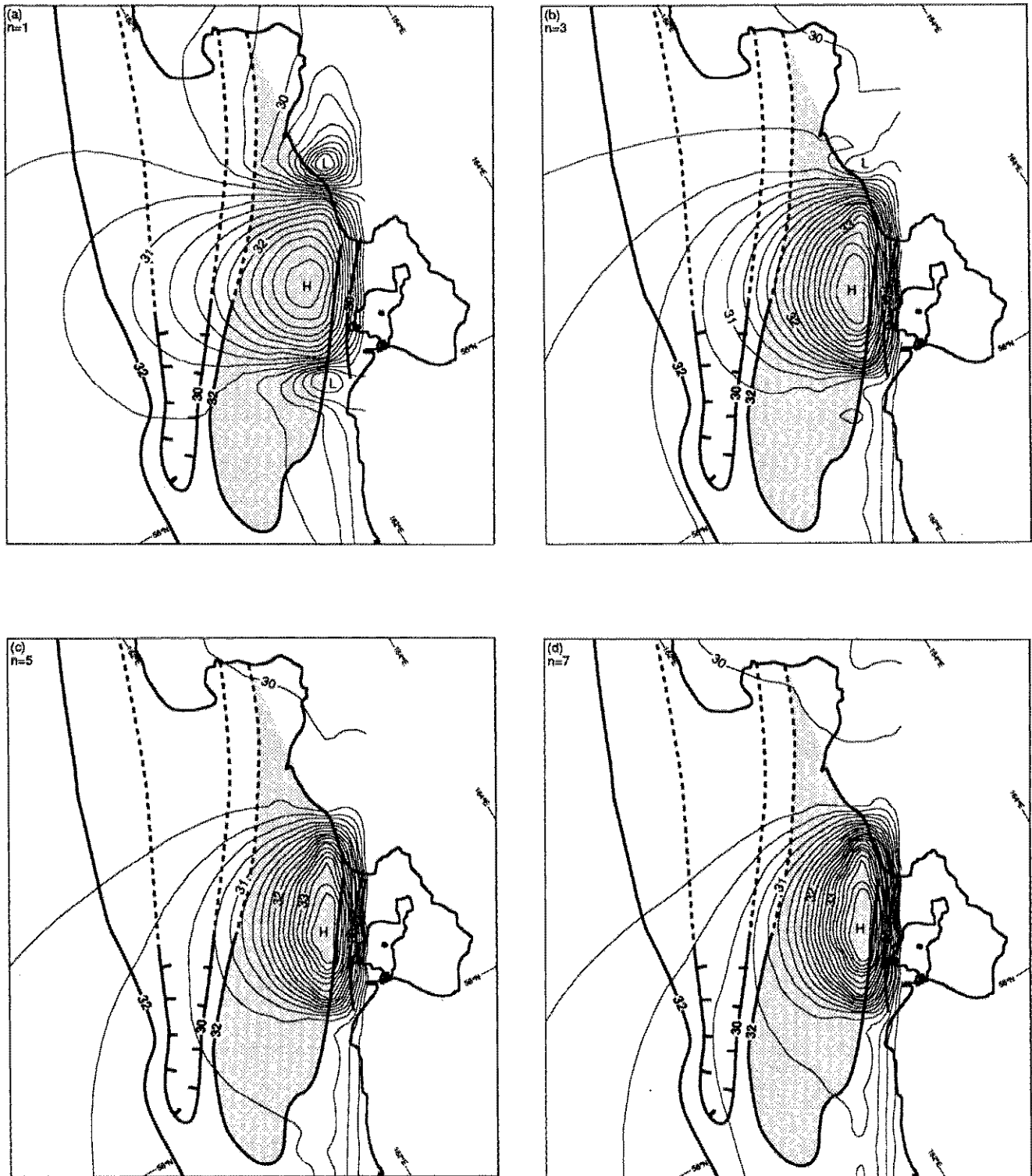


**Figure 12.** Effect on crustal thickness after 5 m.y. by varying  $n$ . Initial thickness is 30 km. Contour interval is 0.2 km. Boundary conditions are same as in Figure 11. Thick contour lines indicate gravimetrically determined crustal thickness [Pavlov and Yunov, 1970]. Lines are dashed where extrapolated based on trends indicated by Gribidenko *et al.* [1974]. Values are (a)  $n=1$ , (b)  $n=3$ , (c)  $n=5$ , and (d)  $n=7$ .

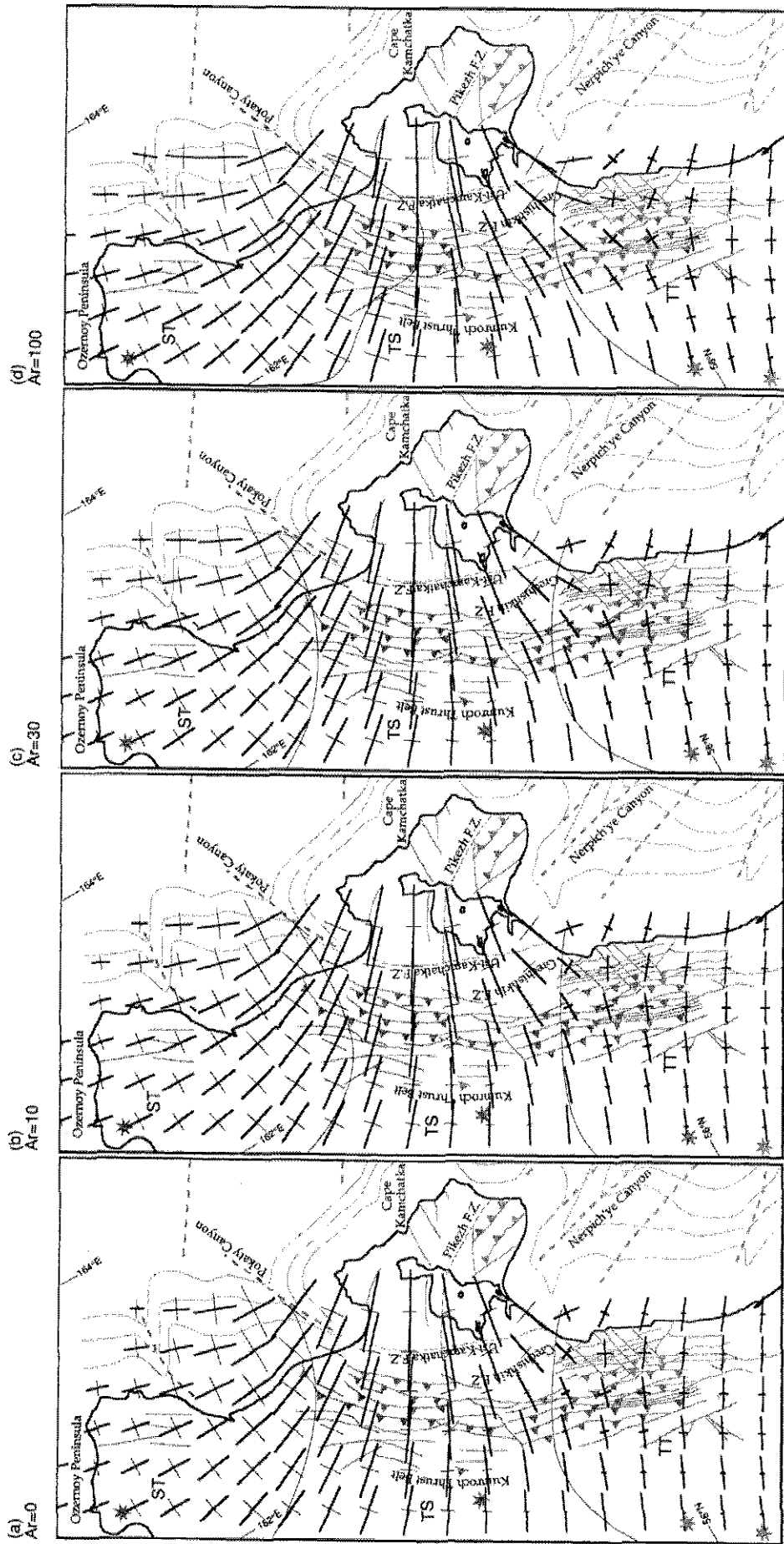
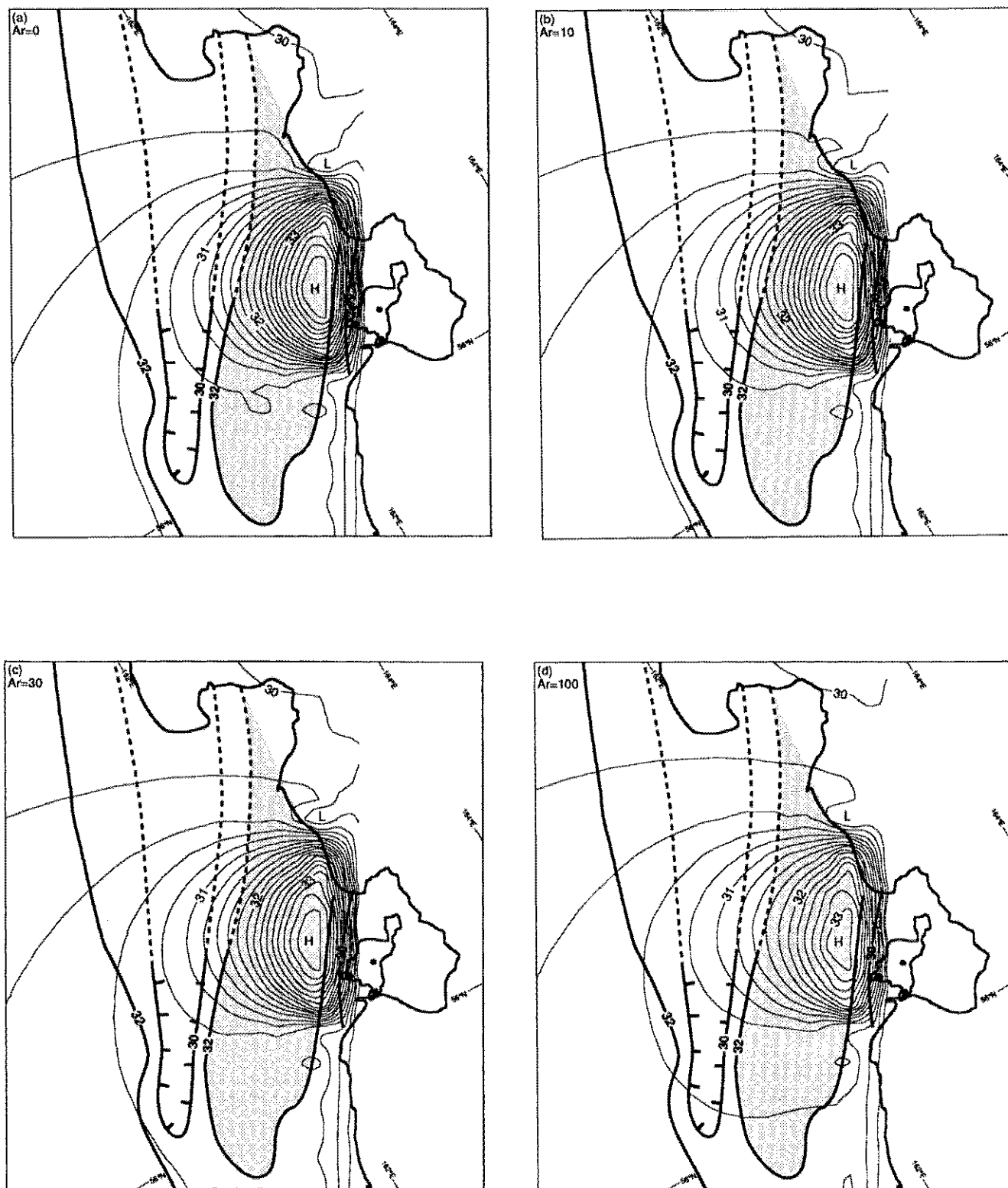
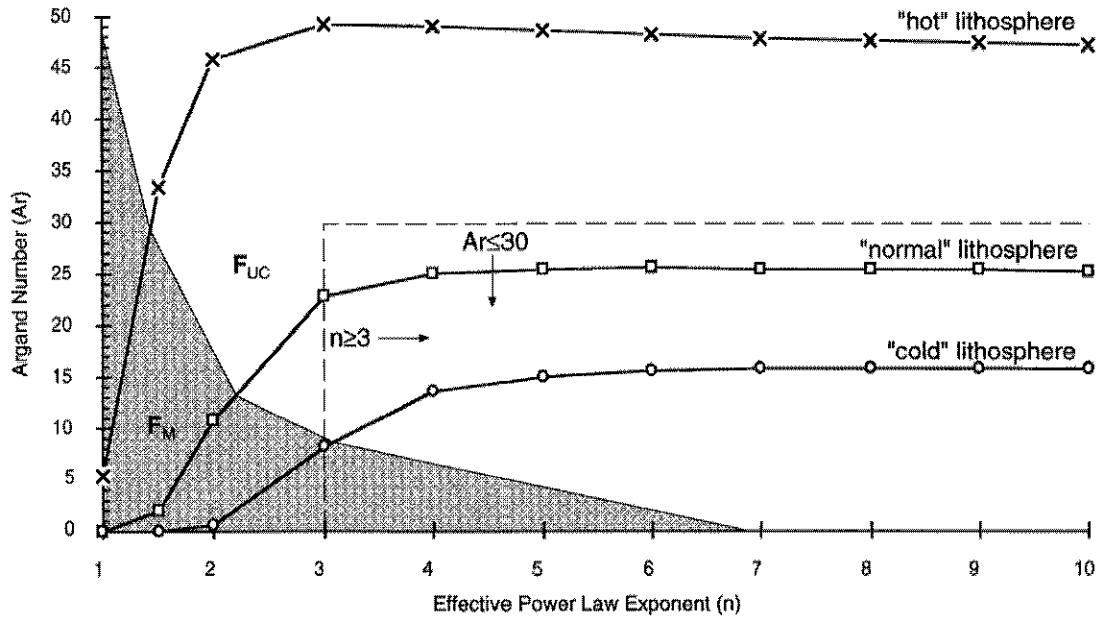


Figure 13. Effect on principal horizontal stresses after 5 m.y. by varying  $A_r$ . Thick axis indicates compressive stress; thin axis indicates tensional stress. Boundary conditions are same as in Figure 10. Values are (a)  $A_r=0$ , (b)  $A_r=10$ , (c)  $A_r=30$ , and (d)  $A_r=100$ .



**Figure 14.** Effect on crustal thickness after 5 m.y. by varying  $Ar$ . Initial thickness is 30 km. Contour interval is 0.2 km. Boundary conditions are same as in Figure 10. Thick contour lines indicate gravimetrically determined crustal thickness [Pavlov and Yunov, 1970]. Lines are dashed where extrapolated based on trends indicated by Gribidenko *et al.* [1974]. Values are (a)  $Ar=0$ , (b)  $Ar=10$ , (c)  $Ar=30$ , and (d)  $Ar=100$ .



**Figure 15.** Effective power law exponent  $n$  versus the Argand number  $Ar$  for three thermal and strength profiles applicable to the Kamchatka subduction zone [Smirnov and Sugrobov, 1980; Sugrobov and Yanovsky, 1993]. Values for  $Ar$  were obtained from equations derived by England [1983] and Sonder and England [1986] by separately estimating the vertically integrated strength of the upper and lower crust and mantle. Dotted area represents region where  $F_M > F_{UC}$ ; unshaded, where  $F_{UC} > F_M$ . Parameters used in the calculations for each of the three cases are listed in Table 3. Optimal ranges of  $n$  and  $Ar$  from modeling results are indicated by dashed lines.

and Sugrobov and Yanovsky [1993]. Likewise,  $T_M$  is determined from the combination of the thermal structure and the crustal structure of Marakhanov and Potap'ev [1981]. The stress difference at the brittle-ductile transition is approximated using curves published by Sibson [1984]. Regions where  $F_{UC} > F_M$  and where  $F_M > F_{UC}$  are also shown in Figure 15.

As expected,  $Ar$  is higher for lithosphere with an elevated thermal structure corresponding to lower vertically integrated strength. As  $n$  increases, the curves approach a constant value of  $Ar$ , representing the dominance of the  $F_{UC}$  term. For very high  $n$  ( $>1000$ , not shown),  $F_{LC}$  increasingly contributes to  $F_L$ , whereas for lower values of  $n$ ,  $F_{LC}$  is insignificant in its contribution to  $F_L$  [Sonder and England, 1986].

Optimal values of  $n \geq 3$  and  $Ar \leq 30$  from deformation modeling correlate with the normal or cold lithosphere in Figure 15. From the Kamchatka thermal data [Smirnov and Sugrobov, 1980, 1982; Sugrobov and Yanovsky, 1993] the normal and cold lithosphere corresponds to the thermal structure of the forearc and trench, while the hot lithosphere corresponds to the arc or back arc (Sea of Okhotsk) thermal structure. The cold lithosphere also corresponds to the thermal structure of the Kamchatka margin north of Cape Kamchatka as determined by Kepezhinskaya [1993]. Thus we can roughly discriminate between primary differences in the thermal structure of the arc lithosphere, although we are unable to identify whether the upper crust or the mantle is the strength-controlling layer (Figure 15). Most likely, both the mantle and upper crust significantly contribute to the strength of

the lithosphere. Interestingly, although there does not seem to exist an expression relating the contribution of the strength of the upper crust to the effective power law exponent, Sonder and England [1986] note that even when the strength of the upper crust and mantle are comparable, a power law relationship is retained. This supports the use of a single power law exponent applicable to the whole lithosphere even though each layer has a different rheology [Sonder and England, 1986].

## Conclusions

Distributed strike-slip motion across the westernmost or Komandorsky segment of the Aleutian Arc results in the collision of arc rocks with the Kamchatka Peninsula. The collision is manifested onshore by a zone of thrust faulting and intense compressional deformation, concave about Cape Kamchatka. The seismogenic contact zone between the Aleutian Arc and Kamchatka seems to be located just offshore of Cape Kamchatka. Active strike-slip and thrust faulting is present offshore, north and south of Cape Kamchatka, as revealed by seismic reflection data and focal mechanisms. Thin viscous sheet modeling indicates that the trend of faults within the Kumroch thrust belt is related to compression from both the collision zone and from sediment-induced coupling of the subducting Pacific plate to the south. The modeling also indicates that strike-slip faulting north

of the collision zone is related to the collision. Comparison of the observed deformation to model results constrain the values of  $n$  and  $Ar$  to  $n \geq 3$  and  $Ar \leq 30$ . Although the range of optimal values that best describes the collision process does not completely constrain the rheology of the continental lithosphere, the values are consistent with a forearc thermal structure.

Many questions regarding the dynamics of the Aleutian Arc-Kamchatka collision are left to be answered. For example, it is unclear if and how the Aleutian Arc is consumed beneath Kamchatka. Also, geological studies to date have not resolved

how far to the west of Cape Kamchatka the Aleutian Arc may have extended. Further understanding of the dynamics of this arc-continent collision will be important in evaluating the seismogenic deformation of this region.

**Acknowledgments.** The authors are grateful to Holly Ryan and Tracy Vallier for early reviews of this manuscript and to Boris Baranov for unpublished geophysical data. We thank *Tectonics* reviewers Eli Silver and Cliff Frohlich for their constructive comments. We also thank Susan Vath for assistance in preparing the figures.

## References

- Artyushkov, E. V., Stresses in the lithosphere caused by crustal thickness inhomogeneities, *J. Geophys. Res.*, **78**, 7675-7708, 1973.
- Ashby, M. F., and R. A. Verrall, Micromechanisms of flow and fracture, and their relevance to the rheology of the upper mantle, *Philos. Trans. R. Soc. London A.*, **288**, 59-95, 1977.
- Baranov, B. V., N. I. Seliverstov, A. V. Murav'ev, and E. L. Muzurov, The Komandorsky Basin as a product of spreading behind a transform plate boundary, *Tectonophysics*, **199**, 237-269, 1991.
- Bazhenov, M. L., V. S. Burtman, O. A., Krezhovskikh, and M. N. Shapiro, Paleomagnetism of Paleogene rocks of the Central-East Kamchatka and Komandorsky Islands: Tectonic implications, *Tectonophysics*, **201**, 157-173, 1992.
- Belyaevsky, N. A., and A. A. Borisov, Deep structure of the northwestern Pacific mobile belt, (in Russian), *Sov. Geol.*, **9**, 29-47, 1964.
- Bird, P., Formation of the Rocky Mountains, western United States: A continuum computer model, *Science*, **239**, 1501-1507, 1988.
- Bird, P., New finite element techniques for modeling deformation histories of continents with stratified temperature-dependent rheology, *J. Geophys. Res.*, **94**, 3967-3990, 1989.
- Borsuk, A. M., A. A. Tsvetkov, D. Z. Zhuravlev, and I. V. Chernyshev, Magmatic evolution of the Kommandorskie Islands in the Aleutian Island Arc, *Geol. Zb. Geol. Carpathica*, **36**, 523-554, 1985.
- Brace, W. F., and D. L. Kohlstedt, Limits on lithospheric stress imposed by laboratory experiments, *J. Geophys. Res.*, **85**, 6248-6252, 1980.
- Buffington, E. C., Aleutian-Kamchatka Trench convergence: An investigation of lithospheric plate interaction in the light of modern geotectonic theory, Ph.D. thesis, 364 pp., Univ. of South. Calif., Los Angeles, 1973.
- Byerlee, J., Friction in rocks, *Pure Appl. Geophys.*, **116**, 615-626, 1978.
- Chapman, M. E., and S. C. Solomon, North American-Eurasian plate boundary in northeast Asia, *J. Geophys. Res.*, **81**, 921-930, 1976.
- Cook, D. B., K. Fujita, and C. A. McMullen, Present-day plate interactions in northeast Asia: North American, Eurasian, and Okhotsk plates, *J. Geodynamics*, **6**, 33-51, 1986.
- Cormier, V. F., Tectonics near the junction of the Aleutian and Kuril-Kamchatka arcs and a mechanism for middle Tertiary magmatism in the Kamchatka Basin, *Geol. Soc. Am. Bull.*, **86**, 443-453, 1975.
- DeMets, C., A test of present-day plate geometries for northeast Asia and Japan, *J. Geophys. Res.*, **97**, 17,627-17,635, 1992.
- DeMets, C., R. G. Gordon, D. F. Argus, and S. Stein, Current plate motions, *Geophys. J. Int.*, **101**, 425-478, 1990.
- Dziewonski, A. M., and J. H. Woodhouse, An experiment in systematic study of global seismicity: Centroid-moment tensor solutions for 201 moderate and large earthquakes of 1981, *J. Geophys. Res.*, **88**, 3247-3271, 1983.
- Dziewonski, A. M., T. A. Chou, and J. H. Woodhouse, Determination of earthquake source parameters from waveform data for studies of global and regional seismicity, *J. Geophys. Res.*, **86**, 2825-2852, 1981.
- Dziewonski, A. M., G. Ekström, and M. P. Salganik, Centroid-moment tensor solutions for October-December 1991, *Phys. Earth Planet. Inter.*, **74**, 89-100, 1992.
- Ekström, G., and E. R. Engdahl, Earthquake source parameters and stress distribution in the Adak Island region of the central Aleutian Islands, Alaska, *J. Geophys. Res.*, **94**, 15,499-15,519, 1989.
- England, P. C., Constraints on extension of continental lithosphere, *J. Geophys. Res.*, **88**, 1145-1152, 1983.
- England, P. C., and G. A. Houseman, Finite strain calculations of continental deformation, 2, Comparison with the India-Asia collision zone, *J. Geophys. Res.*, **91**, 3664-3676, 1986.
- England, P. C., and G. A. Houseman, The mechanics of the Tibetan Plateau, *Philos. Trans. R. Soc. London A.*, **326**, 301-320, 1988.
- England, P. C., and G. A., Houseman, Extension during continental convergence with application to the Tibetan Plateau, *J. Geophys. Res.*, **94**, 17,561-17,579, 1989.
- England, P. C., and D. P. McKenzie, A thin viscous sheet model for continental deformation, *Geophys. J. R. Astron. Soc.*, **70**, 295-321, 1982. (Correction, *Geophys. J. R. Astron. Soc.*, **73**, 523-532, 1983.)
- Fedotov, S. A., A. A. Gusev, G. V. Chernysheva, and L. S. Shumilina, The seismic focal zone of Kamchatka: Geometry, hypocenter distribution, and relation to volcanism, *Volcanol. and Seismol.*, **7**, 593-613, 1988.
- Fedotov, S. A., L. S. Shumilina, and G. V. Chernysheva, The seismicity of Kamchatka and the Komandorsky Islands as revealed by detailed studies, *Volcanol. and Seismol.*, **9**, 861-906, 1990.
- Frohlich, C., Triangle diagrams: Ternary graphs to display similarity and diversity of earthquake focal mechanisms, *Phys. Earth Planet. Inter.*, **75**, 193-198, 1992.
- Frohlich, C., and K. D. Apperson, Earthquake focal mechanisms, moment tensors, and the consistency of seismic activity near plate boundaries, *Tectonics*, **11**, 279-296, 1992.
- Geist, E. L., and D. W. Scholl, Application of continuum models to deformation of the Aleutian island arc, *J. Geophys. Res.*, **97**, 4953-4967, 1992.
- Geist, E. L., J. R. Childs, and D. W. Scholl, The origin of summit basins of the Aleutian Ridge: Implications for block rotation of an arc massif, *Tectonics*, **7**, 327-341, 1988.
- Geist, E. L., M. A. Fisher, and D. W. Scholl, Large-scale deformation associated with ridge subduction, *Geophys. J. Int.*, **115**, 344-366, 1993.
- Geist, E. L., T. L. Vallier, and D. W. Scholl, Origin, transport, and emplacement of an exotic island arc terrane exposed in eastern Kamchatka, Russia, *Geol. Soc. Am. Bull.*, in press, 1994.
- Gnibidenko, H. S., S. Z. Gorbachev, M. M. Lebedev, and V. I. Marakhanov, Geology and deep structure of Kamchatka Peninsula, *Pac. Geol.*, **7**, 1-32, 1974.
- Gnibidenko, H. S., T. G. Bykova, O. V. Veselov, V. M. Vorobiev, and A. S. Svarichevsky, The tectonics of the Kurile-Kamchatka deep-sea trench, in *Geodynamics of the Western Pacific-Indonesian Region*,

- Geodyn. Ser., vol. 11, edited by T. W. C. Hilde and S. Uyeda, pp. 249-285, AGU, Washington, D.C., 1983.
- Goetze, C., The mechanisms of creep in olivine, *Philos. Trans. R. Soc. London A.*, 288, 99-119, 1978.
- Gordeyev, Ye. I., Yu. A. Kugayenko, and V. N. Chebrov, Seismicity on the Kronotskiy Peninsula, *Volcanol. Seismol.*, 13, 345-357, 1992.
- Heiphetz, A., W. Harbert, and L. Savostin, Reconnaissance paleomagnetism of the Olyutorsky superterrane, northeast Russia, paper presented at 1992 International Conference on Arctic Margins, Alaska Geol. Soc., Anchorage, Alaska, in press, 1994.
- Honda, S., Thermal structure beneath Tohoku, northeast Japan--A case study for understanding the detailed thermal structure of the subduction zone, *Tectonophysics*, 112, 69-102, 1985.
- Houseman, G. A., and P. C. England, Finite strain calculations of continental deformation, I. Method and general results for convergent zones, *J. Geophys. Res.*, 91, 3651-3663, 1986.
- Karato, S. I., M. S. Paterson, and J. D. Fitzgerald, Rheology of synthetic olivine aggregates: Influence of grain size and water, *J. Geophys. Res.*, 91, 8151-8176, 1986.
- Kepezhinskas, P., Cold Moho boundary beneath island arc systems: An example from the north Kamchatka arc, *Geophys. Res. Lett.*, 20, 2471-2474, 1993.
- Kirby, S. H., Rheology of the lithosphere, *Rev. Geophys.*, 21, 1458-1487, 1983.
- Kirby, S. H., and A. K. Kronenberg, Rheology of the lithosphere: Selected topics, *Rev. Geophys.*, 25, 1219-1244, 1987.
- Kovalenko, D. V., Tectonic interpretation of paleomagnetic data on island-arc complexes in the Olyutor zone and on Karaginskiy Island, *Geotectonics, Engl. Transl.*, 24, 165-173, 1990.
- Krasny, M. L., K. F. Sergeev, and S. S. Snegovskoy, Seismoacoustic basement surface structure, scale 1:1,500,000, sheet 2, in *Geology-Geophysical Atlas of the Kuril-Kamchatka Island System*, edited by K.F. Sergeev and M.L. Krasny, 21 pp., Minist. Geol., Moscow, 1987.
- Mackwell, S. J., Deformation of fine-grained pyroxenite: Application to lithosphere dynamics, *Eos Trans. AGU*, 73(43) Fall Meeting Suppl., 528, 1992.
- Marakhanov, V. I., and S. V. Potap'ev, *Strukturnoe Raionirovanie Kamchatskoi Tektonicheskoi Oblasti* (The structural zonation of the Kamchatka tectonic region), (in Russian), 87 pp., Nauka, Moscow, 1981.
- Marchenko, A. F., I. A., Sidorchuk, B. V. Lopatin, and T. V. Tarasenko, Geologicheskaya Karta Kamchatskoi Oblasti (Geological map of Kamchatka), scale 1:1,500,000, edited by G. M. Vlasov, Minist. Geol., Moscow, 1976.
- Markov, M. S., V. A. Seliverstov, M. Yu. Khotin, and B. K. Dolmatov, Junction of east Kamchatka structures and the Aleutian Island Arc, *Geotectonics, Engl. Trans.*, 3, 314-319, 1969.
- McCaffrey, R., Oblique plate convergence, slip vectors, and forearc deformation, *J. Geophys. Res.*, 97, 8905-8915, 1992.
- McCaffrey, R., and G. A. Abers, Orogeny in arc-continent collision: The Banda arc and western New Guinea, *Geology*, 19, 563-566, 1991.
- McKenzie, D. P., and J. A. Jackson, The relationship between strain rates, crustal thickening, paleomagnetism, finite strain and fault movements within a deforming zone, *Earth Planet. Sci. Lett.*, 65, 182-202, 1983.
- Muzurov, E. L., B. V. Baranov, Yu. V. Borisenko, P. L. Brudastov, and L. A. Litvinova, Sea-floor spreading in the Komandorsky Basin and structure of the Shirshov Ridge, *Dokl. Acad. Sci. USSR Earth Sci. Sect., Engl. Transl.*, 305, 89-92, 1989.
- Newberry, J. T., D. L. LaClair, and K. Fujita, Seismicity and tectonics of the far western Aleutian Islands, *J. Geodynamics*, 6, 13-32, 1986.
- Pavlov, Yu. A., and A. Yu. Yunov, Thickness of the crust in Kamchatka, *Dokl. Acad. Sci. USSR Earth Sci. Sect., Engl. Transl.*, 191, 38-40, 1970.
- Petrina, N. M., M. N. Shapiro, M. E. Boyarinova, B. I. Slyadnev, A. V. Lander, and V. S. Uspenskie, The upper Cretaceous and lower Paleogene sediments of the eastern ranges of Kamchatka, (in Russian), *Bull. Mosk. Ova. Ispyt. Prir. Otd. Geol.*, 58, 47-61, 1983.
- Ranalli, G., On the possibility of Newtonian flow in the upper mantle, *Tectonophysics*, 108, 179-192, 1984.
- Richardus, P., and R. K. Adler, *Map Projections*, 174 pp., North-Holland, New York, 1972.
- Riegel, S. A., K. Fujita, B. M. Koz'min, V. S. Imaev, and D. B. Cook, Extrusion tectonics of the Okhotsk plate, Northeast Asia, *Geophys. Res. Lett.*, 20, 607-610, 1993.
- Ryan, H. F., and D. W. Scholl, The evolution of forearc structures along an oblique convergent margin, central Aleutian Arc, *Tectonics*, 8, 497-516, 1989.
- Scholl, D. W., J. R. Hein, M. Marlow, and E. C. Buffington, Meiji sediment tongue: North Pacific evidence for limited movement between the Pacific and North American plates, *Geol. Soc. Am. Bull.*, 88, 1567-1576, 1977.
- Scholl, D. W., T. L. Vallier, and A. J. Stevenson, Geologic evolution and petroleum geology of the Aleutian Ridge, in *Geology and Resource Potential of the Continental Margin of Western North America and Adjacent Ocean Basins--Beaufort Sea to Baja California*, *Earth Sci. Ser.*, vol. 6, edited by D. W. Scholl, A. Grantz, and J. G. Vedder, pp. 123-155, Circum-Pacific Council for Energy and Mineral Resources, Houston, Tex., 1987.
- Scholl, D. W., A. J. Stevenson, T. L. Vallier, H. F. Ryan, and E. L. Geist, The Aleutian arc-trench system--A perspective of ocean margin evolution controlled by regional changes in plate-boundary conditions *Proc. Int. Geol. Congr.*, 28th (3), 52-53, 1989.
- Seliverstov, N. I., Structure of junction zone between Kuril-Kamchatka and Aleutian Island Arcs from continuous seismic profiling, *Volcanol. Seismol.*, 5, 175-190, 1984.
- Seliverstov, N. I., *Seismo-akusticheskie Issledovaniia Perekhodnykh Zon*, (in Russian), 112 pp., Nauka, Moscow, 1987.
- Shapiro, M. N., The Grechishkin overthrust on the shores of Kamchatka Gulf, *Geotectonics*, 14, 234-240, 1980.
- Shapiro, M. N., and V. A. Seliverstov, Morphology and age of folded structures in eastern Kamchatka, at the latitude of the Kronotskiy Peninsula, *Geotectonics, Engl. Transl.*, 4, 240-244, 1975.
- Shapiro, M. N., B. I. Slyadnev, and A. V. Lander, Slice-overthrust structure of the northern part of the East Kamchatka Anticlinorium, *Geotectonics, Engl. Transl.*, 18, 514-521, 1984.
- Sibson, R. H., Roughness at the base of the seismogenic zone: Contributing factors, *J. Geophys. Res.*, 89, 5791-5799, 1984.
- Smirnov, Ya. B., and V. M. Sugrobov, Terrestrial heat flow in the Kuril-Kamchatka and Aleutian provinces, III, Assessments of temperature at depth and thickness of the lithosphere, *Volcanol. Seismol.*, 2, 3-18, 1980.
- Smirnov, Ya. B., and V. M. Sugrobov, Terrestrial heat flow in the northwestern Pacific, *Tectonophysics*, 83, 109-122, 1982.
- Smirnov, Ya. B., V. M. Sugrobov, and F. A. Yanovskiy, The terrestrial heat flow of Kamchatka, *Volcanol. Seismol.*, 13, 181-210, 1992.
- Sonder, L. J., and P. C. England, Vertical averages of rheology of the continental lithosphere: Relation to thin sheet parameters, *Earth Planet. Sci. Lett.*, 77, 81-90, 1986.
- Sonder, L. J., and P. C. England, Effects of a temperature-dependent rheology on large scale continental extension, *J. Geophys. Res.*, 94, 7603-7619, 1989.
- Sonder, L. J., P. C. England, and G. A. Houseman, Continuum calculations of continental deformation in transcurrent environments, *J. Geophys. Res.*, 91, 4797-4810, 1986.
- Stauder, W., and L. Mualchin, Fault motion in the larger earthquakes of the Kurile-Kamchatka Arc and of the Kurile-Hokkaido corner, *J. Geophys. Res.*, 81, 297-308, 1976.
- Sugrobov, V. M., and F. A. Yanovskiy, Terrestrial heat flow, estimation of deep

- temperature and seismicity of the Kamchatka region, *Tectonophysics*, 217, 43-53, 1993.
- Suprunenko, O. I., The main faults in east-central Kamchatka, *Dokl. Acad. Sci. USSR Earth Sci. Sect., Engl. Transl.*, 192, 43-45, 1970.
- Suprunenko, O. I., T. A. Andiyeva, and P. N. Safronov, The sublatitudinal Kronoki-Krutogorova fault zone of Kamchatka, *Dokl. Acad. Sci. USSR Earth Sci. Sect., Engl. Transl.*, 209, 92-94, 1973.
- Tarakanov, R. S., Seismicity, distribution of earthquake epicenters, scale 1:3,000,000, in *Geology-Geophysical Atlas of the Kuril-Kamchatka Island System*, edited by K.F. Sergeev and M.L. Krasny, pp. 33-35, Minist. Geol., Moscow, 1987.
- Tsenn, M. C., and N. L. Carter, Upper limits of power law creep of rocks, *Tectonophysics*, 136, 1-26, 1987.
- Tsikunov, A. G., and V. S. Petrov, Overthrust in Vostochny Khrebet (Eastern Range), Kamchatka, *Int. Geol. Rev.*, 15, 208-212, 1973.
- Tsukanov, N. V., and A. V. Fedorchuk, Oceanic complexes in the east Kumroch Range, Kamchatka, *Dokl. Acad. Sci. USSR Earth Sci. Sect., Engl. Transl.*, 307, 99-103, 1989.
- Tsukanov, N. V., and V. P. Zinkevich, The tectonics of the Kumroch Range (eastern Kamchatka), *Geotectonics, Engl. Transl.*, 21, 535-546, 1987.
- Vilotte, J. P., M. Daignières, and R. Madariaga, Numerical modeling of intraplate deformation: Simple mechanical models of continental collision, *J. Geophys. Res.*, 87, 10,709-10,728, 1982.
- Vilotte, J. P., M. Daignières, R. Madariaga, and O. Zienkiewicz, The role of a heterogeneous inclusion during continental collision, *Phys. Earth Planet. Inter.*, 36, 236-259, 1984.
- Vilotte, J. P., R. Madariaga, M. Daignières, and O. Zienkiewicz, Numerical study of continental collision: Influence of buoyancy forces and an initial stiff inclusion, *Geophys. J. R. Astron. Soc.*, 84, 279-310, 1986.
- Watson, B. F., and K. Fujita, Tectonic evolution of Kamchatka and the Sea of Okhotsk and implications for the Pacific Basin, in *Tectonostratigraphic Terranes of the Circum-Pacific Region*, Earth Sci. Ser., vol. 1, edited by D.G. Howell, pp. 333-348, Circum-Pacific Council for Energy and Mineral Resources, Houston, Tex., 1985.
- Wdowinski, S., and R. J. O'Connell, On the choice of boundary conditions in continuum models of continental deformation, *Geophys. Res. Lett.*, 17, 2413-2416, 1990.
- Wdowinski, S., and R. J. O'Connell, Deformation of the central Andes (15°-27°S) derived from a flow model of subduction zones, *J. Geophys. Res.*, 96, 12,245-12,255, 1991.
- Wdowinski, S., R. J. O'Connell, and P. C. England, A continuum model of continental deformation above subduction zones: Application to the Andes and the Aegean, *J. Geophys. Res.*, 94, 10,331-10,346, 1989.
- Weertman, J., Creep laws for the mantle of the Earth, *Philos. Trans. R. Soc. London A*, 288, 9-26, 1978.
- Yogodzinski, G. M., J. L. Rubenstone, S. M. Kay, and R. W. Kay, Magmatic and tectonic development of the western Aleutians: An oceanic arc in a strike-slip setting, *J. Geophys. Res.*, 98, 11,807-11,834, 1993.
- Yoshii, T., Proposal of the "aseismic front", *J. Seismol. Soc. Jpn.*, 28, 365-367, 1975.
- Zinkevich, V. P., O. V. Lyashenko, and V. M. Basmanov, Ophiolite nappes of the Ozernoy Peninsula, eastern Kamchatka, *Dokl. Acad. Sci. USSR Earth Sci. Sect., Engl. Transl.*, 277, 94-97, 1984.
- Zinkevich, V. P., A. D. Kazimirov, A. A. Peyve, and G. M. Churakov, New data on the structure of the Cape Kamchatskiy Peninsula, eastern Kamchatka, *Dokl. Acad. Sci. USSR Earth Sci. Sect., Engl. Transl.*, 285, 89-92, 1985.
- Zobin, V. M., Focal mechanism of shallow and intermediate earthquakes in the Kamchatka-Commander region and heterogeneities of the active seismic zone, *Bull. Volcanol.*, 42, 43-59, 1979.
- Zobin, V. M., Earthquake focal mechanisms and seismotectonic deformation in the Kamchatka-Commander region, *J. Geodynamics*, 12, 1-19, 1990a.
- Zobin, V. M., Consistency of the distribution of foci of earthquakes in the Kamchatka-Komandorsky Islands zone with the double-dipole model, *Dokl. Acad. Sci. USSR Earth Sci. Sect., Engl. Transl.*, 314, 35-37, 1990b.
- Zobin, V. M., The mechanism of earthquake foci and seismotectonic deformation in the Kamchatka-Komandorsky Islands region, 1964-1982, *Volcanol. Seismol.*, 9, 933-955, 1990c.
- Zobin, V. M., Initial rupture and the main fault of earthquakes: A comparison of the body wave first arrivals and CMT data from the Kamchatka-Commander region, *Phys. Earth Planet. Inter.*, 67, 313-329, 1991.
- Zobin, V. M., and I. G. Simbireva, Focal mechanisms of earthquakes in the Kamchatka-Commander region and heterogeneities of the active seismic zone, *Pure Appl. Geophys.*, 117, 283-299, 1977.
- Zobin, V. M., L. K. Ivanenko, and V. N. Chirkova, Seismotectonic deformation of the lithosphere in the Kamchatka-Commander region in the period 1979-1981, *Volcanol. Seismol.*, 8, 595-616, 1990.
- Zonenshain, L. P., M. I. Kuzmin, and L. M. Natapov, *Geology of the USSR: A plate-tectonic synthesis*, *Geodyn. Ser.*, vol. 21, pp. 149-167, 1990.

E. L. Geist and D. W. Scholl, U. S. Geological Survey, 345 Middlefield Road, MS 999, Menlo Park, CA 94025. (e-mail: geist@octopus.wr.usgs.gov; dscholl@octopus.wr.usgs.gov)

(Received October 5, 1993;

revised February 8, 1994;

accepted February 16, 1994.)